Applications of anisotropic polyconvex energies: thin shells and biomechanics of arterial walls

Daniel Balzani, Jörg Schröder, and Patrizio Neff
University Duisburg-Essen, Essen, Germany

Abstract In this contribution a general framework for the construction of polyconvex anisotropic strain energy functions, which a priori satisfy the condition of a stress-free reference configuration, is given. In order to show the applicability of polyconvex functions, two application fields are discussed. First, a comparative analysis of several polyconvex functions is provided, where the models are adjusted to experiments of soft biological tissues from arterial walls. Second, thin-shell simulations, where polyconvex material models are used, show a strong influence of anisotropy when comparing isotropic shells with anisotropic ones.

1 Introduction

With a view to modern engineering applications, very often fiber-reinforced materials are used. Due to the existence of embedded fibers one has to deal with an anisotropic material behavior showing mostly a nonlinear response at large strains. For the modeling of such materials in the sense of continuum mechanics a suitable framework is based on the invariant theory; see e.g. Ericksen and Rivlin (1957) or Doyle and Ericksen (1956) for representations of anisotropic finite elasticity. By introducing structural tensors the polynomial basis of the constitutive equations can be derived in an attractive way. For an introduction to the coordinate-invariant formulation of anisotropic constitutive equations based on the concept of structural tensors we refer to e.g. Spencer (1971), Boehler (1987), or Betten (1987). In order to concretize the general representations of finite elasticity such that a physically reasonable material behavior is obtained, there exist various restrictions to the form of the strain energy. The Coleman-Noll (Coleman and Noll (1959)) inequality implies the convexity of the strain energy with respect to the deformation gradient. In large strain formulations this condition is not reasonable, because it precludes buckling, it is incompatible with the principle

of material frame-indifference and it violates some essential growth requirements. A suitable condition is the Legendre-Hadamard inequality, where the existence of traveling waves is investigated by analyzing the ellipticity of the acoustic tensor. Violation of the Legendre-Hadamard ellipticity leads to material instability of the model and therefore the existence of singular surfaces, which should obviously not occur in the case of hyperelasticity. Furthermore, there exist restrictions on the strain energy with regard to the existence of minimizing deformations of the energy potential under given boundary conditions. In order to ensure the existence of minimizers, the energy has to be coercive and polyconvex in the sense of Ball (1977a,b). This condition can be checked locally and directly implies Legendre-Hadamard ellipticity and therefore material stability. Furthermore, the quasiconvexity condition is a priori satisfied, which ensures that homogeneous bodies do not break down in coexisting stable phases. Anisotropic polyconvex energies, especially for the case of transverse isotropy and orthotropy, have been first introduced by Schröder and Neff (2001, 2003). Extensions and applications of these fundamental functions are documented in Schröder et al. (2005), Itskov and Aksel (2004), Markert et al. (2005), Balzani et al. (2006), Balzani (2006), Ehret and Itskov (2007), and Balzani et al. (2008).
This contribution is organized as follows: after briefly recapitulating essential continuum mechanics in Section 2 a general framework for the generation of polyconvex anisotropic strain energy functions, which automatically satisfy the condition of a stress-free reference configuration, is explained in Section 3. There also numerous polyconvex functions obtained by the given construction principles are derived, which are listed in the appendix. An important application of polyconvex strain energy functions are soft biological tissues since these behave anisotropically and in most cases hyperelastically in a physiological range of deformations. Therefore, this contribution provides a comparative analysis showing the usage of polyconvex functions with respect to these materials in Section 4. Another very important application field of polyconvex functions is the simulation of membrane-like fiber-reinforced lightweight constructions. Several examples showing the influence of anisotropy with respect to such structures are given in Section 5.

2 Continuum-Mechanical Preliminaries

In the (undeformed) reference configuration the body of interest is denoted by $\mathcal{B} \subset \mathbb{R}^3$, parameterized in $\boldsymbol{X}$, and denoted by $\mathcal{S} \subset \mathbb{R}^3$, parameterized in $\boldsymbol{x}$, in the deformed configuration. The nonlinear deformation map $\boldsymbol{\varphi}_t : \mathcal{B} \rightarrow \mathcal{S}$ at time $t \in \mathbb{R}_+$ maps points $\boldsymbol{X} \in \mathcal{B}$ onto points $\boldsymbol{x} \in \mathcal{S}$. The deformation

gradient $\boldsymbol{F}$ and the right Cauchy–Green tensor are defined by

$$\boldsymbol{F}(\boldsymbol{X}) := \mathrm{Grad}[\boldsymbol{\varphi}_t(\boldsymbol{X})] \quad \text{and} \quad \boldsymbol{C} := \boldsymbol{F}^T\boldsymbol{F}\,, \tag{1}$$

with the Jacobian $J := det\,\boldsymbol{F} > 0$. In the case of hyperelastic materials we postulate the existence of a strain-energy function $W(\boldsymbol{F})$, defined per unit reference volume. In order to obtain constitutive equations which satisfy the principle of material objectivity *a priori*, the functional dependence $W(\boldsymbol{F}^T\boldsymbol{F}) = \psi(\boldsymbol{C})$ is taken into account. Then we compute the second Piola–Kirchhoff stresses, the first Pioloa–Kirchhoff stresses and the Cauchy stresses by

$$\boldsymbol{S} = 2\partial_C\psi, \quad \boldsymbol{P} = \boldsymbol{F}\boldsymbol{S} \quad \text{and} \quad \boldsymbol{\sigma} = J^{-1}\boldsymbol{F}\boldsymbol{S}\boldsymbol{F}^T\,, \tag{2}$$

respectively. A suitable framework for the description of anisotropic materials is the concept of structural tensors. Therein, an additional argument tensor, the structural tensor, is defined such that it reflects the symmetry group of the considered material, see e.g. Spencer (1971), Boehler (1987), or Zheng and Spencer (1993). Here we only consider anisotropic materials which can be characterized by certain directions. That means that the anisotropy can be described by some unit vectors $\boldsymbol{A}_{(a)}$ and some second-order tensors $\boldsymbol{M}_{(a)}$ defined in the reference configuration. In the sequel, we concentrate on fiber-reinforced materials, hence, we restrict ourselves to the cases of transverse isotropy and to materials which can be approximated by a given number of superimposed transversely isotropic models. In these cases we are able to express the material symmetry of the considered body by a set of second-order structural tensors

$$\boldsymbol{M}_{(a)} := \boldsymbol{A}_{(a)} \otimes \boldsymbol{A}_{(a)} \quad \text{with} \quad a = 1...n_a\,, \tag{3}$$

where n_a is the number of fiber directions. For the construction of specific constitutive equations we focus on a coordinate-invariant formulation, thus, the invariants of the deformation tensor and of the structural tensors are required. Let $\boldsymbol{M}_{(a)}$ be of rank one and let us assume the normalization condition $||\boldsymbol{M}|| = 1$, then the explicit expressions for the principle and mixed invariants are given by

$$\begin{aligned} &I_1 := \mathrm{trace}\,\boldsymbol{C}, \quad I_2 := \mathrm{trace}[\mathrm{Cof}\boldsymbol{C}], \quad I_3 := \mathrm{det}\boldsymbol{C}, \\ &J_4^{(a)} := \mathrm{trace}[\boldsymbol{C}\boldsymbol{M}_{(a)}], \quad J_5^{(a)} := \mathrm{trace}[\boldsymbol{C}^2\boldsymbol{M}_{(a)}]\,. \end{aligned} \tag{4}$$

For the construction of constitutive equations one obtains the possible polynomial basis

$$\mathcal{P}_{ti} := \{I_1, I_2, I_3, J_4^{(a)}, J_5^{(a)}\}\,. \tag{5}$$

For fiber-reinforced materials, where we assume a weak interaction between the fiber families, the general structure of the strain energy function for a given number of fiber families n_f ends up in

$$\psi(\boldsymbol{C}, \boldsymbol{M}_{(a)}) = \psi^{iso}(I_1, I_2, I_3) + \sum_{a=1}^{n_f} \psi^{ti}_{(a)}(I_1, I_2, I_3, J_4^{(a)}, J_5^{(a)})\,. \tag{6}$$

Herein, the isotropic energy ψ^{iso} describes the behavior of the matrix material, whereas $\psi^{ti}_{(a)}$ represents the energy associated with the response of the fiber family (a). By application of the chain rule one gets

$$\boldsymbol{S} = 2\sum_{i=1}^{5} \frac{\partial \psi}{\partial L_i}\frac{\partial L_i}{\partial \boldsymbol{C}} = \boldsymbol{S}^{iso} + \sum_{a=1}^{n_a} \boldsymbol{S}^{ti}_{(a)} \tag{7}$$

with $L_i \in \mathcal{P}_{ti}$ and the explicit terms for the isotropic and transversely isotropic parts

$$\begin{aligned}
\boldsymbol{S}^{iso} &= 2\left\{\left(\frac{\partial \psi^{iso}}{\partial I_1} + \frac{\partial \psi^{iso}}{\partial I_2} I_1\right)\mathbf{1} - \frac{\partial \psi^{iso}}{\partial I_2}\boldsymbol{C} + \frac{\partial \psi^{iso}}{\partial I_3}\mathrm{Cof}\boldsymbol{C}\right\}, \\
\boldsymbol{S}^{ti}_{(a)} &= 2\left\{\left(\frac{\partial \psi^{ti}_{(a)}}{\partial I_1} + \frac{\partial \psi^{ti}_{(a)}}{\partial I_2} I_1\right)\mathbf{1} - \frac{\partial \psi^{ti}_{(a)}}{\partial I_2}\boldsymbol{C} + \frac{\partial \psi^{ti}_{(a)}}{\partial I_3}\mathrm{Cof}\boldsymbol{C}\right. \\
&\qquad \left. + \frac{\partial \psi^{ti}_{(a)}}{\partial J_4^{(a)}}\boldsymbol{M}_{(a)} + \frac{\partial \psi^{ti}_{(a)}}{\partial J_5^{(a)}}(\boldsymbol{C}\boldsymbol{M}_{(a)} + \boldsymbol{M}_{(a)}\boldsymbol{C})\right\}.
\end{aligned} \tag{8}$$

From the physical point of view it is important to fulfill the condition of a stress-free reference configuration, which can be written down as

$$\boldsymbol{S}(\boldsymbol{C} = \mathbf{1}) = \mathbf{0}\,. \tag{9}$$

Inserting $\boldsymbol{C} = \mathbf{1}$ into the explicit expressions for the second Piola-Kirchhoff stresses given in (8) leads to the side conditions

$$\begin{gathered}
\frac{\partial \psi^{iso}}{\partial I_1} + 2\frac{\partial \psi^{iso}}{\partial I_2} + \frac{\partial \psi^{iso}}{\partial I_3} = 0\,, \\
\frac{\partial \psi^{ti}}{\partial I_1} + 2\frac{\partial \psi^{ti}}{\partial I_2} + \frac{\partial \psi^{ti}}{\partial I_3} = 0\,, \quad \frac{\partial \psi^{ti}_{(a)}}{\partial J_4^{(a)}} + 2\frac{\partial \psi^{ti}_{(a)}}{\partial J_5^{(a)}} = 0\,.
\end{gathered} \tag{10}$$

Herewith, we enforce that $\boldsymbol{S}^{iso}$ vanishes in the natural state independently. At this point it is remarked that especially for polyconvex functions these restrictions are generally not a priori fulfilled.

3 Polyconvexity and Fiber-Reinforced Materials

In the framework of material modeling basic principles as e.g. the principle of material frame indifference or the principle of material symmetry have to be satisfied as well as further restrictions necessary for a mathematically and physically reasonable material behavior. A sufficient condition for the existence of minimizers is the sequential weak lower semicontinuity (s.w.l.s.) of $\int_{\mathcal{B}} W(\boldsymbol{F})\, dV$ on $W^{1,p}(\mathcal{B})$ together with the coercivity of W; $W^{1,p}(\mathcal{B})$ means, that the first derivatives of W exist in the weak sense and are p-times integrable over $\mathcal{B}$.
A condition implying s.w.l.s. is the convexity of the strain energy function with respect to the deformation gradient. Furthermore, a strictly convex function also guarantees the uniqueness of solutions, which means that a local minimum is always a global minimum, too. From the numerical point of view this is quite interesting with view to gradient-based linearization methods. A huge drawback of the convexity condition is that it is physically too restrictive. As an example, convexity of the stored energy precludes buckling and contradicts the principle of material frame indifference. Another important restriction is the quasiconvexity condition, which has been introduced by Morrey (1952) and which represents, together with polynomial growth conditions, a sufficient condition for the s.w.l.s.. Unfortunately, the quasiconvexity condition is an integral inequality and is therefore only conditionally appropriate for the analysis of functions. A more suitable condition for the practical use in this context is the notion of polyconvexity in the sense of Ball (1977b,a), which is a sufficient condition for s.w.l.s. also without growth conditions and which directly implies quasiconvexity. Due to its local character this condition can be checked pointwise. Another important convexity condition is the rank-1-convexity, which is associated with the Legendre-Hadamard ellipticity. In its strong form it ensures wave propagation with real velocity and is strongly linked with material stability. It should be noted that quasiconvexity is a sufficient condition for rank-1-convexity. It is well known that a convex function is also polyconvex, a polyconvex function is also quasiconvex and a quasiconvex function is also rank-1-convex. Generally, the converse implications are not true, see Dacorogna (1989).
Summarizing, the polyconvexity seems to be the most suitable condition since it a priori implies s.w.l.s., which is important for the existence of minimizers, it implies quasiconvexity and rank-1-convexity, which is linked to the physically reasonable requirement of real wave speeds, and it does not preclude some important properties in finite strains like the convexity condition. In order to ensure the existence of minimizers, the polyconvexity

condition alone is not a sufficient one, since it only implies s.w.l.s. but not coercivity. Due to the definition of coercivity we directly notice that each additively composed strain energy with positive additive terms will automatically satisfy the coercivity condition provided that at least one additive term is coercive. It should be noted that in this work we focus on the construction of polyconvex energy functions and do not treat the issue of coercivity for each polyconvex function. The polyconvexity condition reads

Definition of Polyconvexity: $\boldsymbol{F} \mapsto W(\boldsymbol{F})$ *is polyconvex if and only if there exists a function* $P : \mathbb{R}^{3\times3} \times \mathbb{R}^{3\times3} \times \mathbb{R} \mapsto \mathbb{R}$ *(in general non-unique) such that*

$$W(\boldsymbol{F}) = P(\boldsymbol{F}, \mathrm{Cof}[\boldsymbol{F}], \det[\boldsymbol{F}])$$

and the function $\mathbb{R}^{19} \mapsto \mathbb{R}$, $(\tilde{X}, \tilde{Y}, \tilde{Z}) \mapsto P(\tilde{X}, \tilde{Y}, \tilde{Z})$ *is convex for all points* $\boldsymbol{X} \in \mathbb{R}^3$. □

We notice that the arguments of P are exactly the transport theorems for the transition of infinitesimal line-, vectorial area-, and volume elements from the reference to the actual configuration.

3.1 Isotropic Polyconvex Strain Energy Functions

In this section we remember some well-known isotropic functions, which satisfy the polyconvexity condition, cp. Hartmann and Neff (2003), Schröder and Neff (2003). The most straightforward functions are the invariants for the isotropic case themselves, i.e. I_1, I_2 and I_3 as given in (4). The polyconvexity of the third invariant is trivially satisfied, due to the definition of polyconvexity. In order to check the polyconvexity of the first and second invariant we have to prove the convexity of these functions with respect to $\boldsymbol{F}$ and $\mathrm{Cof}[\boldsymbol{F}]$, respectively. For this purpose the second derivative of the functions has to be positive. In order to prove the polyconvexity of positive powers of I_1 we consider the function I_1^k, which can be reformulated by $W(\boldsymbol{F}) = \mathrm{tr}[\boldsymbol{F}^T\boldsymbol{F}]^k = (||\boldsymbol{F}||^2)^k$, and compute the piecewise second derivative. After calculating

$$D_F[W].\boldsymbol{H} = 2k\|\boldsymbol{F}\|^{2k-2}\langle \boldsymbol{F}, \boldsymbol{H}\rangle$$

we obtain the second derivative

$$D_F^2[W].(\boldsymbol{H}, \boldsymbol{H}) = 2k(\|\boldsymbol{F}\|^{2k-2}\langle \boldsymbol{H}, \boldsymbol{H}\rangle + (2k-2)\|\boldsymbol{F}\|^{2k-4}\langle \boldsymbol{F}, \boldsymbol{H}\rangle^2) > 0\,,$$

which is positive for $k \geq 1$. The proof for powers of I_2 is trivially obtained by replacing the cofactor in the derivative. Thus, we obtain the polyconvex functions

$$\psi_1^{iso} = \alpha_1\, I_1^{\alpha_2} \quad \text{and} \quad \psi_2^{iso} = \alpha_1\, I_2^{\alpha_2}\,, \tag{11}$$

with $\alpha_1 > 0$ and $\alpha_2 \geq 1$. For some materials the additive split of the strain energy into a volumetric and an isochoric part is quite important and the energy takes the general form

$$W(\boldsymbol{F}) = W_{vol}(\det[\boldsymbol{F}]) + W_{isoch}(\tilde{\boldsymbol{C}})\,. \tag{12}$$

Herein, we have $\tilde{\boldsymbol{C}} := \det[\boldsymbol{C}]^{-1/3}\,\boldsymbol{C}$, because then the determinant of $\tilde{\boldsymbol{C}}$ is equal to one. For the first invariant of $\boldsymbol{C}$ this means, that the isochoric part is calculated by

$$\tilde{I}_1 = \mathrm{tr}[\tilde{\boldsymbol{C}}] = \frac{I_1}{I_3^{1/3}}\,, \tag{13}$$

whose polyconvexity is proved in e.g. Neff (2000) or Schröder and Neff (2003), Hartmann and Neff (2003). There, it is shown, that the function

$$W(\boldsymbol{F}) = \frac{\|\boldsymbol{F}\|^p}{\det[\boldsymbol{F}]^{\bar{\alpha}}} \quad \text{with} \quad \frac{\bar{\alpha}+1}{\bar{\alpha}} \geq \frac{p}{p-1} \tag{14}$$

is a polyconvex function. This holds for the case $\bar{\alpha} = 2/3$ and $p = 2$, which is associated with the function given in (13). The substitution of $\|\boldsymbol{F}\|$ by $\|\mathrm{Cof}[\boldsymbol{F}]\|$ in (14) would lead to the analogous proof of polyconvexity for the function $W(\boldsymbol{F}) = \det[\boldsymbol{F}]^{-\bar{\alpha}}\|\mathrm{Cof}[\boldsymbol{F}]\|^p$. Unfortunately, for the isochoric part of I_2 the parameters would be $\bar{\alpha} = 4/3$ and $p = 2$, which would not satisfy the condition $(\bar{\alpha}+1)/\bar{\alpha} \geq p/(p-1)$. Reformulated in direct terms of the invariants we obtain the polyconvex functions

$$\psi_3^{iso} = \alpha_1 \frac{I_1}{I_3^{1/3}} \quad \text{and} \quad \psi_4^{iso} = \alpha_1 \frac{I_2}{I_3^{1/3}} \tag{15}$$

with $\alpha_1 > 0$. For volumetric energy functions formulated in I_3 some polyconvex functions are given by

$$\psi_5^{iso} = \alpha_1\, I_3^{\alpha_2} \quad \text{and} \quad \psi_6^{iso} = -\alpha_1 \ln(I_3) \tag{16}$$

with $\alpha_1 > 0$ and $\alpha_2 > 1 \vee \alpha_2 < 0$. Due to $I_3 = (\det\boldsymbol{F})^2 > 0$ the second derivative of the power function in $(16)_1$ is always positive and therefore polyconvex. The same holds for the second function in (16), because the negative natural logarithm is a monotonically increasing function.
Although the functions given above satisfy the polyconvexity condition, they have a physical drawback: they themselves do not fulfill the condition of a stress-free reference configuration, which is an important requirement for material models. Therefore, we now recapitulate some isotropic polyconvex functions that satisfy this natural state condition. In Hartmann and Neff

functions that satisfy this natural state condition. In Hartmann and Neff (2003), Schröder and Neff (2003) some examples for such functions are given

$$\begin{aligned}
\psi_7^{iso} &= \alpha_1 \left(I_3^{\alpha_2} + \frac{1}{I_3^{\alpha_2}} - 2 \right)^{\alpha_3} && , \quad \alpha_1 > 0, \;\; \alpha_2 \geq \alpha_3 \geq 1 \,, \\
\psi_8^{iso} &= \alpha_1 \left(I_3^{\frac{1}{2}} - 1 \right)^{\alpha_2} && , \quad \alpha_1 > 0, \;\; \alpha_2 \geq 1 \,, \\
\psi_9^{iso} &= \alpha_1 \left(\frac{I_1^{\alpha_2}}{I_3^{\alpha_2/3}} - 3^{\alpha_2} \right)^{\alpha_3} && , \quad \alpha_1 > 0, \;\; \alpha_2 \geq 1 \;\; \alpha_3 \geq 1 \,, \\
\psi_{10}^{iso} &= \alpha_1 \left(\frac{I_2^{3\alpha_2/2}}{I_3^{\alpha_2}} - (3\sqrt{3})^{\alpha_2} \right)^{\alpha_3} && , \quad \alpha_1 > 0, \;\; \alpha_2 \geq 1 \;\; \alpha_3 \geq 1 \,.
\end{aligned} \tag{17}$$

For the proof of polyconvexity we refer to Hartmann and Neff (2003), where the coercivity issue is also investigated for special isotropic energies. For further functions see the Appendix. In the context of the description of soft biological tissues the function

$$\psi_{11}^{iso} = \alpha_1 \left(\frac{I_1}{I_3^{1/3}} - 3 \right) , \; \alpha_1 > 0 \,, \tag{18}$$

is often utilized in the literature, as for example in Holzapfel et al. (2000), Holzapfel et al. (2004a) and similarly in Weiss et al. (1996). Another function for the isotropic part of soft biological tissues is

$$\psi_{12}^{iso} = \alpha_1 \left(\frac{I_2}{I_3^{1/3}} - 3 \right) , \; \alpha_1 > 0 \,. \tag{19}$$

The difference between the latter two functions is the usage of I_1 and I_2 and therewith the use of the terms in $\boldsymbol{C}$ and in Cof$\boldsymbol{C}$, respectively.

3.2 Fundamental Transversely Isotropic Polyconvex Functions

In this section the fundamental polyconvex functions for transverse isotropy as introduced in Schröder and Neff (2003) are briefly recapitulated. For a more extensive description see the contribution of Schröder in this book. As in the previous section we firstly investigate the invariants for transverse isotropy themselves, because these would be the most straightforward functions. When reformulating $J_4 = \mathrm{tr}[\boldsymbol{CM}] = \boldsymbol{FA} : \boldsymbol{FA} = \|\boldsymbol{FA}\|^2$ one obtains the polyconvex functions

$$\psi_1^{ti} = \alpha_1 \, J_4^{\alpha_2} \quad \text{and} \quad \psi_2^{ti} = \alpha_1 \, \frac{J_4^{\alpha_2}}{I_3^{1/3}} \tag{20}$$

with $\alpha_1 > 0$ and $\alpha_2 \geq 1$. For the proof of polyconvexity see Schröder and Neff (2003). Please note that from now on we skip the index $(\bullet)_{(a)}$ if ideal transverse isotropy with only one preferred direction is treated. It is to be remarked that the function ψ_2 for $\alpha_2 = 1$ represents the isochoric part $\tilde{J}_4$ of the fourth invariant, thus, it might be a useful function for volumetrically-isochorically decoupled models. By utilizing an alternative structural tensor the construction of further fundamental functions is possible based on the introduction of

$$K_2 = \mathrm{tr}[\boldsymbol{C}(\boldsymbol{1} - \boldsymbol{M})] = I_1 - J_4\,, \tag{21}$$

see Schröder and Neff (2003), and one obtains the polyconvex functions

$$\psi_3^{ti} = \alpha_1\, K_2^{\alpha_2} \quad \text{and} \quad \psi_4^{ti} = \alpha_1\, \frac{K_2^{\alpha_2}}{I_3^{1/3}} \tag{22}$$

with $\alpha_1 > 0$ and $\alpha_2 \geq 1$. Since the functions J_4 and K_2 are linear in $\boldsymbol{C}$ and therefore possess a relatively limited mapping range, the supply of quadratic terms in $\boldsymbol{C}$ seems to be profitable. Unfortunately, it turns out that the fifth invariant $J_5 = \mathrm{tr}[\boldsymbol{C}^2\boldsymbol{M}]$ is not polyconvex, see Merodio and Neff (2006), although the associated isotropic basic invariant $J_2 = \mathrm{tr}[\boldsymbol{C}^2]$ is polyconvex. A variety of transversely isotropic polyconvex functions is based on the introduction of the function

$$K_1 = \mathrm{tr}[\mathrm{cof}[\boldsymbol{C}]\boldsymbol{M}] = J_5 - I_1\, J_4 + I_2\,, \tag{23}$$

which is a polyconvex function with non-polyconvex terms J_5 and $I_1\, J_4$. After a short algebraic transformation we obtain $K_1 = ||\mathrm{Cof}[\boldsymbol{F}]\boldsymbol{A}||^2$ and see that $\sqrt{K_1}$ controls the change of area with a unit normal vector into the preferred direction $\boldsymbol{A}$. Due to this physical interpretation, K_1 seems to be a suitable function for the description of transverse isotropy. By replacing the structural tensor $\boldsymbol{M}$ in K_1 by the alternative one, we obtain the additional polyconvex function

$$K_3 = \mathrm{tr}[\mathrm{Cof}[\boldsymbol{C}](\boldsymbol{1} - \boldsymbol{M})] = I_1\, J_4 - J_5\,. \tag{24}$$

When reformulating $K_3 = \|\mathrm{Cof}[\boldsymbol{F}]\|^2 - \|\mathrm{Cof}[\boldsymbol{F}]\boldsymbol{A}\|^2$ we notice that $\sqrt{K_3}$ controls the deformation of an area element with a normal vector perpendicular to the preferred direction $\boldsymbol{A}$. Analogous to the proof of polyconvexity for (20) we obtain the polyconvex functions

$$\psi_5^{ti} = \alpha_1\, K_1^{\alpha_2}\,,\ \psi_6^{ti} = \alpha_1\, \frac{K_1^{\alpha_2}}{I_3^{1/3}}\,,\ \psi_7^{ti} = \alpha_1\, K_3^{\alpha_2} \text{ and } \psi_8^{ti} = \alpha_1\, \frac{K_3^{\alpha_2}}{I_3^{1/3}} \tag{25}$$

with $\alpha_1 > 0$ and $\alpha_2 \geq 1$. In Schröder and Neff (2003) a variety of further polyconvex functions constructed by additive combinations of polyconvex and non-polyconvex terms are introduced.

3.3 Polyconvex Framework for Anisotropic Functions Satisfying a priori the Natural State Condition

Regrettably, the functions given in the last section do not satisfy the stress-free reference configuration (9). To overcome this problem one can construct suitable additive combinations of individual polyconvex functions and then derive restrictions with respect to material parameters from (10) in order to satisfy the natural state condition. Although this is in general possible it is not a really generous approach. However, a first polyconvex transversely isotropic function constructed in this fashion is proposed in Schröder and Neff (2001), see also Schröder et al. (2005) for two fiber families. A more elegant additive combination is proposed in Itskov and Aksel (2004), see also Ehret and Itskov (2007) and Schröder et al. (2008) for a more general form. However, in order to be more flexible, e.g. when only a moderate number of material parameters should be used for the approximation of highly nonlinear problems, an alternative approach is proposed in Balzani (2006), see also Balzani et al. (2006). There, a principle for the simple construction of polyconvex energy functions that automatically satisfy the condition of a stress-free reference configuration is given motivated by the fact that a function $\mathbb{R}^n \mapsto \mathbb{R}, X \mapsto m(P(X))$ is convex, if the function $P : \mathbb{R}^n \mapsto \mathbb{R}$ is convex and the function $m : \mathbb{R} \mapsto \mathbb{R}$ is convex and monotonically increasing, cp. Schröder and Neff (2003), Lemma B.9. The principle can be rephrased in words as the following problem:

> *Principle 1a: find a polyconvex function $P(X)$ which is zero in the reference configuration and include this function into any arbitrary convex and monotonically increasing function m, whose first derivative with respect to P vanishes in the origin; then the polyconvex function satisfying the stress-free reference configuration is given by $\psi = m(P(X))$.*

Convex and monotonically increasing functions whose first derivative with respect to P is equal to zero could be

$$m_1(P) = P^k \quad \text{and} \quad m_2(P) = \cosh(P) - 1 \tag{26}$$

with $P \geq 0$ and $k > 1$. The requirement for positive internal functions $P \geq 0$ means that we have to consider the case distinction

$$m = \begin{cases} m(P) & \text{for} \quad P > 0 \\ 0 & \text{for} \quad P \leq 0\,. \end{cases} \tag{27}$$

This seems to be a suitable approach, because $P = 0$ represents the referential state and therefore, we obtain a smooth energy function when satisfying

$m(P = 0) = 0$. A result of introducing the case distinction (27) may be that discontinuous stress functions and/or discontinuous tangent moduli are obtained. Therefore, we investigate m_1 and m_2 with respect to their first and second derivatives. In a first investigation we consider the power function $\psi = m_1$ and compute the first derivative with respect to the (inner) polyconvex function P

$$\partial_P \psi = k\, P^{k-1} \quad \text{with} \quad k > 1\,. \tag{28}$$

We notice that (28) vanishes at the reference configuration since P is equal to zero at the natural state. Hence, also the second Piola–Kirchhoff stresses

$$\boldsymbol{S} = 2\,\partial_C \psi = 2\,\partial_P \psi \sum_{L_i \in \mathcal{P}} \frac{\partial P}{\partial L_i} \frac{\partial L_i}{\partial \boldsymbol{C}} \quad \text{with} \quad L_i \in \mathcal{P} \tag{29}$$

are zero in the reference configuration and the case distinction leads to a continuous stress function. Please note that at this point $\mathcal{P}$ can be an arbitrary polynomial basis describing any type of anisotropy. Then we calculate the second derivative

$$\partial^2_{PP} \psi = k\,(k-1)\, P^{k-2} \quad \text{with} \quad k > 2 \tag{30}$$

and observe that the tangent moduli

$$\mathbb{C} = 2\partial_C \boldsymbol{S} = 4\,\partial^2_{PP}\psi \frac{\partial P}{\partial \boldsymbol{C}} \otimes \sum_{L_i \in \mathcal{P}} \frac{\partial P}{\partial L_i} \frac{\partial L_i}{\partial \boldsymbol{C}} + 4\,\partial_P \psi \frac{\partial}{\partial \boldsymbol{C}} \left[\sum_{L_i \in \mathcal{P}} \frac{\partial P}{\partial L_i} \frac{\partial L_i}{\partial \boldsymbol{C}} \right] \tag{31}$$

are also equal to zero in the reference configuration for $k > 2$ since the first and second derivatives of P are zero in the natural state. Therefore, the tangent moduli are continuous for $k > 2$, too, when the case distinction (27) is considered.
Now we focus on the hyperbolic cosine and set $\psi = m_2$. The first derivative of this energy function with respect to P is given by

$$\partial_P \psi = \sinh(P) \tag{32}$$

and we see that $\partial_P \psi$ vanishes for $P = 0$. Hence, the stresses are zero in the reference configuration and the case distinction (27) leads to a continuous stress function. By computing the second derivative

$$\partial^2_{PP} \psi = \cosh(P) \tag{33}$$

we notice that (33) is not zero for $P = 0$ and therefore, it is not guaranteed that the tangent moduli vanish in the reference configuration. This would

lead to discontinuous tangent moduli at $P = 0$ when the case distinction (27) is considered.

Due to the fact, that a convex and monotonically increasing function $m(P(X))$, whose first derivative with respect to P vanishes in the origin, has a global minimum in the origin, we can reformulate Principle 1a as

> *Principle 1b: find a polyconvex function $P(X)$ which is zero in the reference configuration and include this function into any arbitrary convex and monotonically increasing function m, which attains its global minimum in the origin; then the polyconvex function satisfying the stress-free reference configuration is given by $\psi = m(P(X))$.*

In order to give an example we consider the strain energy function of the cosine hyperbolic type as proposed in (26), i.e.

$$\psi_{cosh} = \begin{cases} \cosh(P) - 1 & \text{for} \quad P \geq 0 \\ 0 & \text{for} \quad P < 0\,. \end{cases} \tag{34}$$

As (inner) functions P which satisfy the condition of an energy-free reference configuration we can use any polyconvex function describing any type of anisotropy. In order to obtain an energy-free referential state, which is also a physically convenient condition, constant factors that have the value of the function itself in the reference configuration have to be subtracted, i.e. $\psi = m(P) - m(P = 0)$. For the case of isotropy or transverse isotropy we are able to include the polyconvex functions given in the sections before, provided that a suitable constant factor $m(P = 0)$ is subtracted.
In addition to the functions obtained by applying Principle 1, we are able to construct further polyconvex functions a priori ensuring the stress-free reference configuration. Analogously motivated by the fact that a function $\mathbb{R}^n \mapsto \mathbb{R}, X \mapsto g(m(X))$ is convex, if the function $m : \mathbb{R}^n \mapsto \mathbb{R}$ is convex and the function $g : \mathbb{R} \mapsto \mathbb{R}$ is convex and monotonically increasing we obtain the principle:

> *Principle 2: include any function $m(P(X))$, obtained by applying Principle 1, into the exponential function $g(m) = exp(m)$; then further polyconvex functions are given by*
>
> $$\psi = \begin{cases} exp(m(P(X))) & for \quad P \geq 0 \\ 0 & for \quad P < 0\,. \end{cases}$$

Due to the fact that the stresses are computed by replacing ψ in the right hand side of (29) by m and multiplying the formula by the derivative $\partial_m \psi$

the stresses governed by Principle 2 are also zero in the referential state. Analogously, the properties with respect to continuous tangent moduli of the functions $\psi = m_1$ or $\psi = m_2$ are preserved.

3.4 Transversely Isotropic Polyconvex Strain Energy Functions

Now we are interested in constructing transversely isotropic polyconvex functions by utilizing the construction principles given above. As a first function we choose the strain energy function

$$\psi^{ti}_{(P1)} = \alpha_1 \langle J_4 - 1 \rangle^{\alpha_2} \tag{35}$$

with $\alpha_1 \geq 0$ and $\alpha_2 > 1$. Herein, the Macauley bracket $\langle(\bullet)\rangle := \frac{1}{2}[|(\bullet)| + (\bullet)]$ filters out positive values. This function fits into the first construction principle, because $P = J_4 - 1$ is polyconvex and $(...)^p$ is convex and monotonically increasing for positive convex arguments. For the complete proof of convexity see Balzani et al. (2006). At the referential state the internal function J_4 takes the value 1, therefore, it is subtracted here in order to normalize P. It should be noted that setting $\alpha_2 > 2$ leads to continuous tangent moduli as shown in the previous section. Due to the fact that J_4 represents the square of the stretch in fiber direction $\boldsymbol{A}$ the distinction of cases in (35), expressed by the Macauley bracket, seems to be reasonable, because $J_4 < 1$ characterizes the shortening of the fibers, which is assumed not to generate stresses. Note that replacing J_4 by its isochoric part $\tilde{J}_4 = J_4 / I_3^{1/3}$ leaves (35) polyconvex provided that the case-distinction is adapted accordingly. Soft biological tissues are characterized by an exponential-type stress-strain behavior in the fiber direction. A model for the description of these materials, which also satisfies the condition of a stress-free reference configuration, is proposed by Holzapfel et al. (2004a, 2000). The transversely isotropic function appears as

$$\psi^{ti}_{(HGO)} = \frac{k_1}{2k_2} \left\{ \exp\left[k_2 \langle J_4 - 1 \rangle^2 \right] - 1 \right\} , \tag{36}$$

where $k_1 \geq 0$ is a stress-like and $k_2 > 0$ a dimensionless material parameter. An appropriate choice of k_1 and k_2 enables the histologically-based assumption that the collagen fibers do not influence the mechanical response of the artery in the low pressure domain to be modeled, see Roach and Burton (1957). The proof of convexity of (36) with respect to $\boldsymbol{F}$ is, e.g., given in Schröder et al. (2005), see also Balzani et al. (2006). Note that the replacement of J_4 by its isochoric part $\tilde{J}_4$ is also possible without violating the convexity condition. Additionally note that the natural state condition is satisfied. We see, that this function fits into the second principle, because

$m = k_2\langle J_4 - 1\rangle^2$ fits into the first principle as already shown above and is embedded into the exponential function as proposed in Principle 2. Since the function $\exp[k_2\langle J_4 - 1\rangle^2]$ is equal to one at the natural state, 1 is subtracted to satisfy the (not necessary) condition of an energy-free reference configuration. The replacement of J_4 in (36) and (35) by an arbitrary polyconvex function leads to a large number of polyconvex functions, which are listed in the Appendix.

As examples we construct some special transversely isotropic polyconvex functions. Since the functions given in (35) and (36) are based on invariants that are linear in $\boldsymbol{C}$, and therefore have a relatively limited mapping range, the use of quadratic terms in $\boldsymbol{C}$ would be profitable. By using the function K_1 we are able to construct two more strain-energy functions which satisfy the condition of a stress-free reference configuration a priori, i.e.

$$\psi^{ti}_{(P2)} = \alpha_1\langle K_1 - 1\rangle^{\alpha_2} \quad \text{and} \quad \psi^{ti}_{(P3)} = \frac{\alpha_1}{2\alpha_3}\left\{\exp\left[\alpha_3\langle K_1 - 1\rangle^2\right] - 1\right\} \tag{37}$$

with $\alpha_1 \geq 0$, $\alpha_2 > 1$ and $\alpha_3 > 0$. Please note, that $\alpha_2 > 2$ ensures continuous tangent moduli. The first function ($\psi^{ti}_{(P2)}$) represents the substitution of J_4 by K_1 in (35), while the second one characterizes a slight modification in the model of Holzapfel, Gasser & Ogden. The proof of polyconvexity for (37) is straightforward, since a convex and monotonically increasing function of a polyconvex argument is also polyconvex (Schröder and Neff (2003)). K_1 and also K_2 control the change of area with a unit normal into the preferred direction in some sense, thus, in a uniaxial tension test of an incompressible material these two functions increase if the material is shortened. Therefore, any function containing K_1 or K_2, that is governed by the given construction principle (e.g., the functions (37) generate stresses mainly when the material is shortened in the preferred direction. This is physically not meaningful for soft biological tissues since collagen fibers mainly support tensile stresses. Nevertheless, it might be useful for some cases to activate stresses under such a condition; then functions like (37) may be utilized.

For incompressible materials K_3 increases when the material is elongated in the direction $\boldsymbol{A}$. Hence, using K_3 for the construction of further polyconvex strain energy functions is physically meaningful for soft biological tissues, because then stresses are generated when the fibers are elongated. As examples we obtain the two strain-energy functions

$$\psi^{ti}_{(P4)} = \alpha_1\langle K_3 - 2\rangle^{\alpha_2} \quad \text{and} \quad \frac{\alpha_1}{2\alpha_3}\left\{\exp\left[\alpha_3\langle K_3 - 2\rangle^2\right] - 1\right\} \tag{38}$$

with $\alpha_1 \geq 0$, $\alpha_2 > 1$ and $\alpha_3 > 0$. These functions are also polyconvex, the proof of which is analogous to (37). It is remarked that setting $\alpha_2 > 2$ leads

to continuous tangent moduli. Of course other polyconvex functions can be obtained by replacing J_4, K_1 and K_3 with any other polyconvex function. An extensive list of polyconvex functions governed by this way is given in the Appendix. It is worth noting that every other monotonically increasing function, e.g., also the other function given in (26), cosh(...), with positive and polyconvex arguments would lead to a polyconvex function, too. As an example, if the function proposed by Rüter and Stein (2000)

$$\psi^{ti}_{(P6)} = \alpha_1 \cosh\langle J_4 - 1\rangle \,, \tag{39}$$

was embedded, then this would provide a polyconvex function.

4 Polyconvex Energies Applied to Biomechanics

In this section we focus on some special three-dimensional constitutive models for healthy elastic arterial tissues, which are mainly composed of a groundsubstance and embedded collagen fibers. It is well-known, that biological tissues adapt to loading conditions in order to obtain an optimized state, e.g. the fibers are usually arranged in such a way that the load can be resisted in an optimal way. As examples in ligaments or tendons the fibers are basically oriented in one direction while the collagen fibers in arterial walls are mainly oriented in two directions forming two crosswise arranged helixes. In order to represent the above explained characteristics we consider a strain energy function of the structure as given in Eq. (6) and set $n_f = 2$. Then, the groundsubstance is described by the isotropic part ψ^{iso} and the fibers by the superposition of the transversely isotropic parts $\psi^{ti,(a)}$ for each of the two fiber orientations. In the previous section a variety of transversely isotropic polyconvex functions are constructed based on the construction principle given there. These functions require to take into account a special case distinction, but have the great advantage that they themselves satisfy the condition of a stress-free reference configuration automatically. To give an example of the applicability of these energy functions some suitable models are adjusted to the Media (the middle layer of the artery) of a human carotid artery.

4.1 Experimental Data for a Human Carotid Artery

The Media of a human carotid artery, which has been excised during autopsy within 24 hours after death is analyzed. The arterial wall was separated anatomically into the three layers, i.e. Intima, Media and Adventitia. Here, we focus on the Media, because from the mechanical perspective the Media is the most significant layer in a healthy artery. From the Media, strip

samples with axial and circumferential orientations were cut out so that two specimens were obtained. For representative tissue samples see, for example, Fig. 4 in Holzapfel et al. (2004b)). Prior to testing, pre-conditioning was achieved by executing five loading and unloading cycles for each test to obtain repeatable stress-strain curves. Subsequently, the stripes underwent uniaxial extension tests in 0.9 % NaCl solution at 37°C with continuous recording of tensile force, strip width and gage length. For details on the customized tensile testing machine the reader is referred to Schulze-Bauer et al. (2002). Additional experimental data for uniaxial extension tests for the Intima, Media and Adventitia of human abdominal aortas are given in Holzapfel (2006).

4.2 Method for Parameter Adjustment

In this section we deduce the equations necessary for the evaluation of general anisotropic material laws for the specific boundary conditions defined by the experiments. As already mentioned, in arteries we observe mainly two fiber families oriented crosswise, thus we assume that the fibers are oriented as shown in Fig. 1. Then the associated structural tensors are computed by

$$\boldsymbol{M}_{(1)} = \begin{bmatrix} s^2 & -cs & 0 \\ -cs & c^2 & 0 \\ 0 & 0 & 0 \end{bmatrix} \quad \text{and} \quad \boldsymbol{M}_{(2)} = \begin{bmatrix} s^2 & cs & 0 \\ cs & c^2 & 0 \\ 0 & 0 & 0 \end{bmatrix} \tag{40}$$

for the extension test in circumferential direction. Herein, the abbreviations $c := \cos(\beta_f)$ and $s := \sin(\beta_f)$ are inserted.

We focus on uniaxial extension tests and assume an incompressible material behavior. Therefore, the coefficients of the deformation gradient and the right Cauchy-Green tensor are written in terms of the stretch in extension direction λ_1 and the transverse stretch in the fiber plane λ_2, i.e.

$$\boldsymbol{F} = \begin{bmatrix} \lambda_1 & 0 & 0 \\ 0 & \lambda_2 & 0 \\ 0 & 0 & \lambda_1^{-1}\lambda_2^{-1} \end{bmatrix} \quad \text{and} \quad \boldsymbol{C} = \begin{bmatrix} \lambda_1^2 & 0 & 0 \\ 0 & \lambda_2^2 & 0 \\ 0 & 0 & \lambda_1^{-2}\lambda_2^{-2} \end{bmatrix}. \tag{41}$$

In order to incorporate incompressibility an additional penalty term is included in the strain energy function such that the structure of the overall energy function reads

$$\tilde{\psi} := \psi + p(I_3 - 1) \quad \text{where} \quad \psi = \psi^{iso} + \sum_{a=1}^{2} \psi^{ti}_{(a)}\,, \tag{42}$$

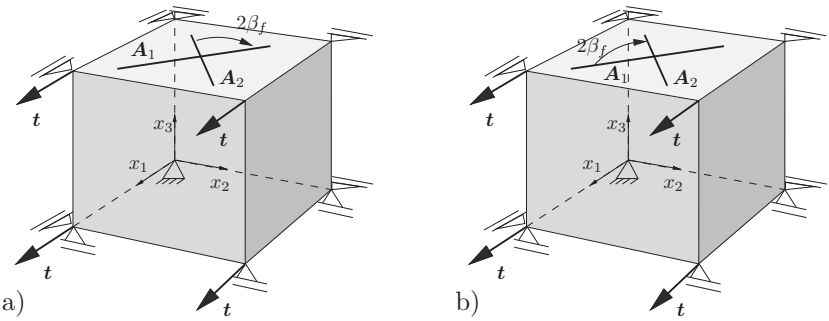

Figure 1: Uniaxial extension in a) circumferential and b) axial direction of a test stripe taken from an artery. Note that the fiber angle β_f describes the angle between the circumferential and the fiber direction.

which is a suitable polyconvex strain energy function describing the material behavior of the soft biological tissue and p is a Lagrange multiplier. Please note that ψ needs not necessarily to be isochoric. Following Eq. (2) we obtain the general constitutive equation

$$\boldsymbol{S} = 2\left(\frac{\partial \psi}{\partial \boldsymbol{C}} + p\,\mathrm{Cof}[\boldsymbol{C}]\right). \tag{43}$$

Taking into account the symmetry of the experiments $\psi^{ti} := \psi^{ti}_{(1)} = \psi^{ti}_{(2)}$ and Eq. $(41)_1$ one finds that

$$\begin{aligned} S_{22} \;=\; & 2\left\{\frac{\partial \psi^{iso}}{\partial I_1} + \frac{\partial \psi^{iso}}{\partial I_2}\left(\lambda_1^2 + \lambda_1^{-2}\lambda_2^{-2}\right) + \left(p + \frac{\partial \psi^{iso}}{\partial I_3}\right)\lambda_2^{-2}\right. \\ & +2\left[\frac{\partial \psi^{ti}}{\partial I_1} + \frac{\partial \psi^{ti}}{\partial I_2}\left(\lambda_1^2 + \lambda_1^{-2}\lambda_2^{-2}\right)\right. \\ & \left.\left. +\frac{\partial \psi^{ti}}{\partial I_3}\lambda_2^{-2} + \frac{\partial \psi^{ti}}{\partial J_4^{(a)}}s^2 + \frac{\partial \psi^{ti}}{\partial J_5^{(a)}}2\lambda_2^2 s^2\right]\right\} = 0\,. \end{aligned} \tag{44}$$

From this equation we are able to compute the Lagrange multiplier p, which is then inserted into the requirement $S_{33} = 0$ in order to obtain a relation

between the first and second stretch λ_1 and λ_2

$$\begin{aligned} S_{33} &= 2\left(\frac{\partial\psi^{iso}}{\partial I_1}\left(1-\lambda_1^2\lambda_2^4\right)+\frac{\partial\psi^{iso}}{\partial I_2}\left(\lambda_1^2-\lambda_1^4\lambda_2^4\right)\right. \\ &\quad +2\left[\frac{\partial\psi^{ti}}{\partial I_1}\left(1-\lambda_1^2\lambda_2^4\right)+\frac{\partial\psi^{ti}}{\partial I_2}\left(\lambda_1^2-\lambda_1^4\lambda_2^4\right)\right. \\ &\quad \left.\left.-\frac{\partial\psi^{ti}}{\partial J_4^{(a)}}\lambda_1^2\lambda_2^4 s^2-2\frac{\partial\psi^{ti}}{\partial J_5^{(a)}}\lambda_1^2\lambda_2^6 s^2\right]\right)=0\,. \end{aligned} \tag{45}$$

It is obvious that this equation can not be solved analytically for the general case, thus, a Newton-scheme is used. For this purpose we consider the linearization

$$\mathrm{Lin}S_{33}=S_{33}^{(i)}+\left(\frac{\partial S_{33}}{\partial\lambda_2}\right)^{(i)}\Delta\lambda_2^{(i+1)}=0\,, \tag{46}$$

where the index $(\bullet)^{(i)}$ and $(\bullet)^{(i+1)}$ denote values at the last and at the actual iteration step, respectively. The iteration is repeated, where in each step the increment $\Delta\lambda_2$ is computed and updated $\lambda_2^{(i+1)} \Leftarrow \lambda_2^{(i)}+\Delta\lambda_2^{(i+1)}$, until the stresses vanish ($S_{33} < tol$). As the starting value in each iteration procedure we set $\lambda_1^{(0)}$ equal to the extension stretch of interest, i.e. to the value measured in the experiment. In order to improve the efficiency of the iteration we consider the modified starting value for

$$\lambda_2^{(0)} := \tilde{\lambda}_2\sqrt{\frac{\tilde{\lambda}_1}{\lambda_1^{(0)}}}\,, \tag{47}$$

wherein the quantities $(\tilde{\bullet})$ denote quantities resulting from the last iteration procedure. With this method in hand we are able to compute the only stress in x_1-direction S_{11} governed by a general hyperelastic constitutive model as a function of the stretch λ_1 read from the experiment. In order to be able to compare the computed stresses with the experimental ones the Cauchy stresses have to be calculated by $\sigma_{comp}=\lambda_1^2\,S_{11}$. Then we define the relative error

$$r(\lambda_1,\boldsymbol{\alpha}) := \frac{|\sigma_{exp}(\lambda_1)-\sigma_{comp}(\lambda_1,\boldsymbol{\alpha})|}{\max[\sigma_{exp}]}\,, \tag{48}$$

wherein the normalization by the maximum value of experimental stresses in the considered extension cycle $\max[\sigma_{exp}] \neq 0$ is introduced. The vector $\boldsymbol{\alpha}$ contains all material parameters involved in the constitutive energy ψ. For the adjustment higher values of experimental stresses are highlighted,

thus, the resulting total error, which now deals as an objective function,

$$\bar{r}(\boldsymbol{\alpha}) = \sum_{e=1}^{n_e} \sqrt{\frac{1}{n_{mp}} \sum_{m=1}^{n_{mp}} \left(\frac{\sigma_{exp}(\lambda_1^{(m)}) - \sigma_{comp}(\lambda_1^{(m)}, \boldsymbol{\alpha})}{\max[\sigma_{exp}]} \right)^2} \tag{49}$$

is minimized by use of a sequential quadratic programming algorithm. Here, we consider the number of $n_e = 2$ experiments: extension in circumferential and axial direction. The number of measuring points is $n_{mp} = 49$ for the axial and $n_{mp} = 43$ for the circumferential extension test.

4.3 Comparative Analysis of Polyconvex Models

As a first example we consider the model of Balzani et al. (2006), which consists of the polyconvex isotropic part Eq. (18) and the polyconvex transversely isotropic part Eq. $(38)_1$. Then the complete energy is given by

$$\psi^0_{BNSH} = c \left(I_1 \, I_3^{-1/3} - 3 \right) + \sum_{a=1}^{2} \alpha_1 \left\langle K_3^{(a)} - 2 \right\rangle^{\alpha_2} . \tag{50}$$

Herein, c and α_1 scale the isotropic and transversely isotropic response, respectively, and α_2 is a parameter determining the degree of the exponential character of the model. Please note that the fiber angle β_f, defined as the angle between the circumferential and the fiber directions, is also treated as a fitting parameter and not identified from microscopic analysis. The parameters for the best fit to the experimental data are shown in Table 1, where we notice a total relative error of $\bar{r} = 0.126$. The fiber angle results to be $\beta_f = 9.2°$.

	c	α_1	α_2	β_f	$\bar{r}$
	[kPa]	[kPa]	[-]	[°]	[-]
ψ^0_{BNSH}	8.85	23995.25	3.06	40.14	0.126

Table 1: Parameters of the model ψ^0_{BNSH}.

The stress-stretch response of the experimental and the constitutive model is depicted in Fig. 2a for the circumferentially and axially oriented strip whereas Fig. 2b shows the progress of the relative error r during extension. We observe a good agreement for the axially oriented strip and a slight deviation from the experiments with view to the axial one. This is also expressed by the higher relative errors shown in Fig. 2b.

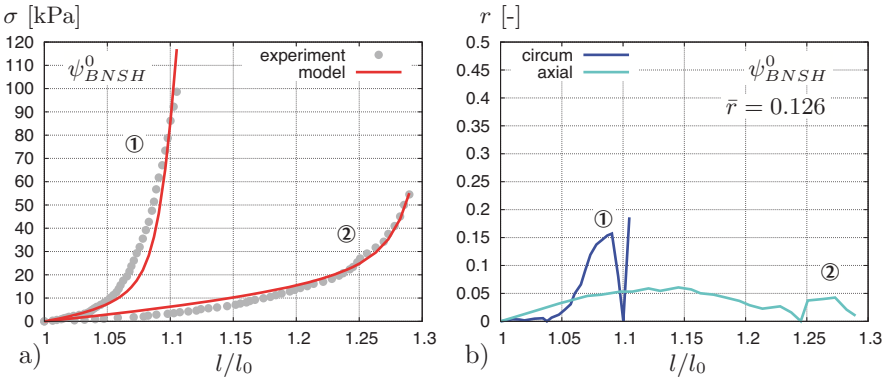

Figure 2: a) Stress-stretch response and b) relative error in uniaxial extension tests of a Media strip oriented in circumferential ① and axial direction ② for the strain energy ψ^0_{BNSH}.

In order to improve the constitutive model the most straightforward way could be to replace the anisotropic part in Eq. (6) by a series of anisotropic parts, then the energy is structured as

$$\psi = \psi^{iso} + \sum_{s=1}^{n_s} \sum_{a=1}^{n_f} \psi^{ti}_{(s,a)} \,, \tag{51}$$

where n_s is the number of series parts taken into account. Note that this ansatz is motivated by the well-known Ogden approach, which has also been addapted by Itskov and Aksel (2004). With view to the polyconvex energy given in Eq. (50) we are able to write down the improved model

$$\psi^s_{BNSH} = c\left(I_1\, I_3^{-1/3} - 3\right) + \sum_{s=1}^{n_s} \sum_{a=1}^{2} \alpha_1^{(s)} \left\langle K_3^{(a,s)} - 2 \right\rangle^{\alpha_2^{(s)}} . \tag{52}$$

We set $n_s = 2$ and adjust the model to the experiments, then we obtain the parameters shown in Table 2 and the stress-stretch response depicted in Fig. 3a.

Now, a good correlation with the experiments is observed, which is also shown by the lower curves of the relative error, see Fig. 3b. The total relative error $\bar{r} = 0.0840$ is much lower than the error obtained for ψ^0_{BNSH}, thus, we conclude a better response of ψ^s_{BNSH}, although the micromechanical motivation for the consideration of two additional anisotropic energies with differing fiber orientations remains questionable.

	c [kPa]	s	α_1 [kPa]	α_2 [-]	β_f [°]	κ [-]	$\bar{r}$ [-]
ψ^s_{BNSH}	8.52	1	2974.06	2.42	40.07	–	0.084
		2	6501.06	11.83	30.25	–	
ψ^κ_{BNSH}	7.54		984.29	2.18	39.48	0.06	0.036

Table 2: Material parameters of the models ψ^s_{BNSH} and ψ^κ_{BNSH}.

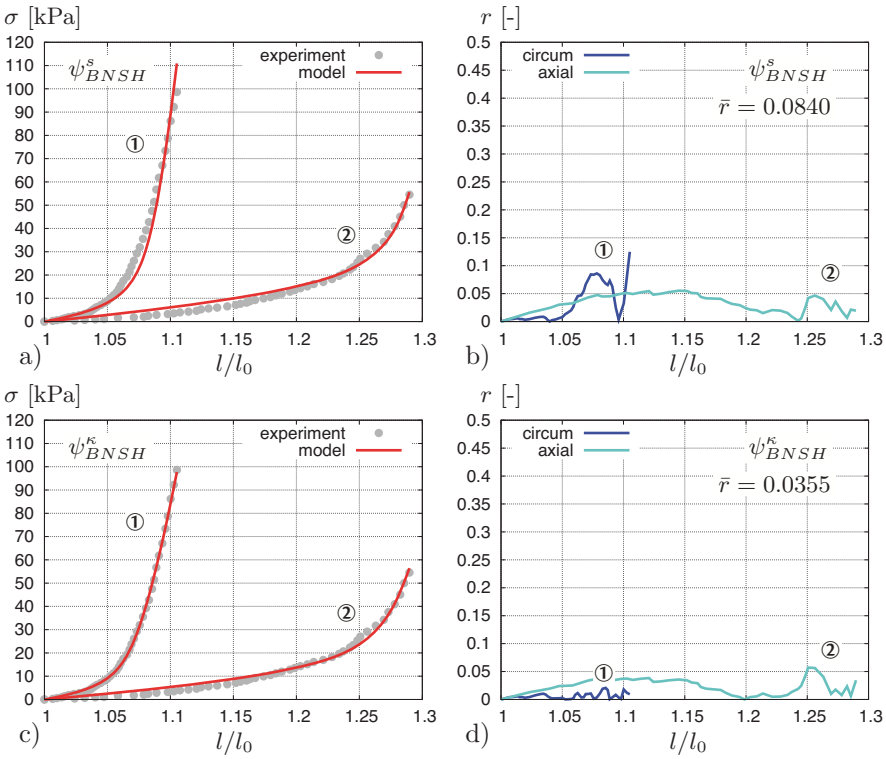

Figure 3: a,c) Stress-stretch response and b,d) relative error in uniaxial extension tests of a Media strip oriented in circumferential ① and axial direction ② for the strain energies ψ^s_{BNSH} and ψ^κ_{BNSH}, respectively.

A more physically interpretable improvement of the model Eq. (50) can be obtained by taking into account that fibers are not ideally oriented in one direction. By including a special internal function following the idea of the fiber dispersion approach used in Gasser et al. (2006) we end up in the energy function

$$\psi^{\kappa}_{BNSH} = c\left(I_1\, I_3^{-1/3} - 3\right) + \sum_{a=1}^{2} \alpha_1 \left\langle \kappa I_1 + \left(1 - \frac{3}{2}\kappa\right) K_3^{(a)} - 2 \right\rangle^{\alpha_2}. \quad (53)$$

Herein, the additional parameter $\kappa \in [0, 2/3]$ scales between an isotropic distribution of the fibers ($\kappa = 2/3$) and an anisotropic fiber distribution ($\kappa = 0$). Please note that since the additive terms I_1 and K_3 form a polyconvex internal function, the resulting function Eq. (53) will also be a polyconvex function. If we now fit this model to the experiments and treat the parameter κ as a fitting parameter which is not identified from microscopical analysis, then we obtain the parameters as given in Table 2.

Again, we observe a good aggreement with the experiments when comparing the stress-stretch response of the model with the experiment shown in Fig. 3c, see also Fig. 3d for the curves of the relative errors. Furthermore, we again conclude an even better response than for the model Eq. (52) since the total error $\bar{r} = 0.0355$ is even lower than the half of the total error of Eq. (52).

Since $K_3 = I_1\, J_4 - J_5$ takes into account a quadratic mixed invariant of $\boldsymbol{C}$ ($J_5 = \mathrm{tr}[\boldsymbol{C}^2\boldsymbol{M}]$) and it also incorporates a term coupling the isotropic response with the fiber elongation ($I_1\, J_4$), this function seems to be appropriate to describe a wide range of fiber-reinforced materials. With view to soft biological tissues, where we can assume a relatively weak interaction between the ground substance and the fibers, the incorporation of J_4 into the transversely isotropic energy may be sufficient. In addition, the fourth mixed invariant $J_4 = \mathrm{tr}[\boldsymbol{C}\boldsymbol{M}] = \lambda_f^2$ has the advantage that it describes the square of the fiber stretch λ_f and hence, provides a clear micromechanical interpretation. For this reason we analyze the often used and well-known transversely isotropic function of Holzapfel, Gasser & Ogden, cp. Eq. (36), and consider again the additive improvement given in Eq. (51). Then the complete polyconvex energy function reads

$$\begin{aligned} \psi^{s}_{HGO} &= c\left(I_1\, I_3^{-1/3} - 3\right) \\ &+ \sum_{s=1}^{n_s} \sum_{a=1}^{2} \frac{k_{1(s)}}{2k_{2(s)}} \left\{ exp\left[k_{2(s)} \left\langle J_4^{(a,s)} - 1 \right\rangle^2 \right] - 1 \right\}. \end{aligned} \quad (54)$$

The parameter c scales the isotropic response whereas k_1 and k_2 are parameters for the fiber behavior. Again we set $n_s = 2$ and adjust the model to

the experiments. Then the material parameters result in the ones listed in Table 3.

	c [kPa]	s	k_1 [kPa]	k_2 [-]	β_f [°]	κ [-]	r [-]
ψ^s_{HGO}	1.18	1	1312.95	390.58	27.46	–	0.03707780
		2	16.38	31.57	54.74	–	
ψ^κ_{HGO}	7.3		1482.38	564.81	37.02	0.16	0.03724851

Table 3: Material parameters for the models ψ^s_{HGO} and ψ^κ_{HGO}.

By comparing the stress-stretch response of the model with the experiments and analyzing the relative errors depicted in Fig. 4a and Fig. 4b, respectively, we notice a good correlation. The total error $\bar{r} = 0.0371$ is even lower than the one of the model ψ^s_{BNSH}.

Now we consider the model Eq. (36) and incorporate a similar ansatz for the fiber distribution as in Eq. (53), then we write down the energy function

$$\begin{aligned} \psi^\kappa_{HGO} &= c\left(I_1\, I_3^{-1/3} - 3\right) \\ &+ \sum_{a=1}^{2} \frac{k_1}{2k_2}\left\{ exp\left[k_2\left\langle \kappa I_1 + (1-3\kappa)J_4^{(a)} - 1\right\rangle^2\right] - 1\right\}, \end{aligned} \tag{55}$$

with $\kappa \in [0, 1/3]$. Please note that due to the fact that the additive terms I_1 and J_4 form a polyconvex internal function and thus, as a result of the construction principles given in section Eq. 3 the complete energy is polyconvex. The model is adjusted to the experiments again and the material parameters listed in Table 3 are obtained. Interestingly, a very similar fiber angle $\beta_f = 37.02°$ compared to the one of ψ^κ_{BNSH} is computed. The stress-stretch response of the model and the relative errors are depicted in Fig. 4c and Fig. 4d, respectively. It can be observed that the model fits the experiment with high accuracy and also the total error $\bar{r} = 0.0372$ is comparable to the one of ψ^κ_{BNSH} or ψ^s_{HGO}.

Concluding this section, we note that it seems to be necessary to include a fiber distribution into the models in order to obtain a good representation of the material behavior. Although the improvements due to the incorporation of anisotropic polyconvex function series (ψ^s_{BNSH} and ψ^s_{HGO}) have been remarkable, we emphasize the relatively clear micromechanical interpretation of the fiber splay approaches used in ψ^κ_{BNSH} and ψ^κ_{HGO}. Both functions are relatively simple, their parameters have a direct meaning with

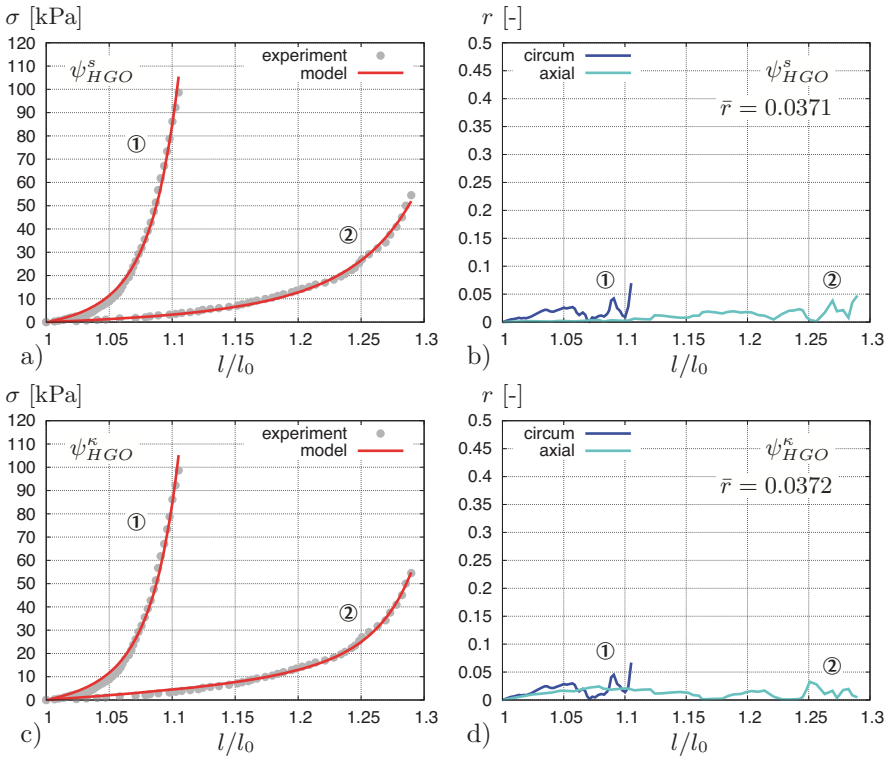

Figure 4: a,c) Stress-stretch response and b,d) relative error in uniaxial extension tests of a Media strip oriented in circumferential ① and axial direction ② for the strain energies ψ^s_{HGO} and ψ^κ_{HGO}, respectively.

respect to the mechanical response and they are polyconvex, thus, they seem to be suitable for the description of soft biological tissues.

5 Application of Polyconvex Energies to Thin Shells

In the following we analyze the influence of anisotropy in membrane-like materials. Such structures are often composed of woven fiber networks made of glass-, textile- or synthetic fibers, embedded in a silicone-, polymer- or rubberlike matrix. Therefore, we apply some of the polyconvex functions obtained by the construction principles in Section 3 capable to describe such fiber-reinforced materials to thin shell problems. *The following results are mainly based on a common work with F. Gruttmann* (Balzani, Gruttmann & Schröder (2008)).

5.1 Thin Shell Kinematics

In the reference configuration the shell body is parametrized in $\boldsymbol{\Phi}$ and in the current configuration in $\boldsymbol{\phi}$. The nonlinear deformation map $\boldsymbol{\varphi}_t : \mathcal{B} \rightarrow \mathcal{S}$ at time $t \in \mathbb{R}_+$ maps points $P \in \mathcal{B}$ onto points of $\mathcal{S}$. With ξ^i we introduce a convected coordinate system of the shell, where ξ^3 is the thickness coordinate with $-h/2 \leq \xi^3 \leq h/2$. Here, h denotes the thickness and the mid-surface Ω is defined by $\xi^3 = 0$. A director field $\boldsymbol{D}(\xi^1, \xi^2)$ is defined as a vector perpendicular to Ω. In the sequel the usual summation convention is used, where Latin indices range from 1 to 3 and Greek indices range from 1 to 2. The position vector $\boldsymbol{\Phi}$ of any point $P \in \mathcal{B}$ is defined by

$$\boldsymbol{\Phi}(\xi^1, \xi^2, \xi^3) = \boldsymbol{\Phi}^i \, \boldsymbol{e}_i = \boldsymbol{X} + \xi^3 \, \boldsymbol{D}(\xi^1, \xi^2) \quad \text{with} \quad |\boldsymbol{D}(\xi^1, \xi^2)| = 1 \tag{56}$$

and $-h/2 \leq \xi^3 \leq h/2$, where $\boldsymbol{X}(\xi^1, \xi^2)$ denotes the position vector of the shell mid–surface Ω. Hence, the geometry of the deformed shell space is described by

$$\boldsymbol{\phi}(\xi^1, \xi^2, \xi^3) = \boldsymbol{\phi}^i \, \boldsymbol{e}_i = \boldsymbol{x}(\xi^1, \xi^2) + \xi^3 \, \boldsymbol{d}(\xi^1, \xi^2) \quad \text{with} \quad |\boldsymbol{d}(\xi^1, \xi^2)| = 1 \,. \tag{57}$$

The inextensible director $\boldsymbol{d}$ is obtained by applying an orthogonal transformation to the initial vector $\boldsymbol{D}$. Since $\boldsymbol{d}$ is not normal to the current configuration the kinematic assumption (57) allows transverse shear strains. The deformation gradient $\boldsymbol{F}$ is then defined by $\mathbf{F}(\boldsymbol{\Phi}) := \nabla \boldsymbol{\varphi}_t(\boldsymbol{\Phi})$ with the Jacobian $J(\boldsymbol{\Phi}) := det\, \mathbf{F}(\boldsymbol{\Phi}) > 0$. The right Cauchy Green tensor is then computed by Eq. $(1)_2$. Next, the Green–Lagrangean strain tensor with covariant components E_{ij} and contravariant basis $\boldsymbol{G}^i$ is given by

$$\boldsymbol{E} = \frac{1}{2}(\boldsymbol{C} - \mathbf{1}) = E_{ij} \, \boldsymbol{G}^i \otimes \boldsymbol{G}^j \,, \qquad E_{ij} = \frac{1}{2}(\boldsymbol{\phi}_{,i} \cdot \boldsymbol{\phi}_{,j} - \boldsymbol{\Phi}_{,i} \cdot \boldsymbol{\Phi}_{,j}) \,. \tag{58}$$

Please note that commas denote partial derivatives with respect to the coordinates ξ^i. Inserting the equations (56) and (57) into $(58)_2$ yield

$$E_{\alpha\beta} = \varepsilon_{\alpha\beta} + \xi^3 \, \kappa_{\alpha\beta} + (\xi^3)^2 \, \rho_{\alpha\beta} \quad \text{and} \quad 2\, E_{\alpha 3} = \gamma_\alpha \,. \tag{59}$$

Note that E_{33} will be computed iteratively in a scheme where the stresses in thickness direction vanish, cp. Section 5.3. In (59) the membrane strains $\varepsilon_{\alpha\beta}$, curvatures $\kappa_{\alpha\beta}$ and shear strains γ_α are given by

$$\begin{aligned} \varepsilon_{\alpha\beta} &= \frac{1}{2}(\boldsymbol{x}_{,\alpha}\cdot\boldsymbol{x}_{,\beta}-\boldsymbol{X}_{,\alpha}\cdot\boldsymbol{X}_{,\beta})\,, \\ \kappa_{\alpha\beta} &= \frac{1}{2}(\boldsymbol{x}_{,\alpha}\cdot\boldsymbol{d}_{,\beta}+\boldsymbol{x}_{,\beta}\cdot\boldsymbol{d}_{,\alpha}-\boldsymbol{X}_{,\alpha}\cdot\boldsymbol{D}_{,\beta}-\boldsymbol{X}_{,\beta}\cdot\boldsymbol{D}_{,\alpha})\,, \\ \gamma_\alpha &= \boldsymbol{x}_{,\alpha}\cdot\boldsymbol{d}-\boldsymbol{X}_{,\alpha}\cdot\boldsymbol{D}\,. \end{aligned} \tag{60}$$

The shell strains are organized in the vector

$$\boldsymbol{\varepsilon} = [\varepsilon_{11},\varepsilon_{22},2\varepsilon_{12},\kappa_{11},\kappa_{22},2\kappa_{12},\gamma_1,\gamma_2]^T\,, \tag{61}$$

wherein the second order curvatures $\rho_{\alpha\beta}$ are neglected for thin structures.

5.2 Variational form of the Shell Formulation

The present finite element formulation is based on a three field variational functional introduced by Simo and Rifai (1990) in the context of small strain elasticity and plasticity. Geometrical nonlinear extentions of the method have been presented in Simo and Armero (1992) using enhanced displacement gradients. Here we follow the approach for nonlinear shells in Betsch et al. (1996), where the shell strains $\boldsymbol{\varepsilon}$ are enhanced by $\hat{\boldsymbol{\varepsilon}} = \boldsymbol{\varepsilon} + \tilde{\boldsymbol{\varepsilon}}$. The shell is loaded statically by surface loads $\bar{\boldsymbol{p}}$ on Ω and by boundary forces $\bar{\boldsymbol{t}}$ on the boundary Γ_σ. The variational framework for the enhanced assumed strain method is the three field variational functional in a Lagrangean representation

$$\Pi(\boldsymbol{v},\tilde{\boldsymbol{\varepsilon}},\tilde{\boldsymbol{\sigma}}) = \int\limits_{(\Omega)} [W(\hat{\boldsymbol{\varepsilon}}(\boldsymbol{v})) - \tilde{\boldsymbol{\sigma}}^T\tilde{\boldsymbol{\varepsilon}}]\,dA - \int\limits_{(\Omega)} \boldsymbol{u}^T\bar{\boldsymbol{p}}\,dA - \int\limits_{(\Gamma\sigma)} \boldsymbol{u}^T\,\bar{\boldsymbol{t}}\,ds \tag{62}$$

with $dA = j\,d\xi^1\,d\xi^2$ and $j = |\,\boldsymbol{X}_{,1}\times\boldsymbol{X}_{,2}|$. The first term describes the internal potential, while the last two terms denote the potential of the external forces. Here, $\boldsymbol{v} = [\boldsymbol{u}^T,\boldsymbol{\omega}^T]^T$, $\tilde{\boldsymbol{\varepsilon}}$, and $\tilde{\boldsymbol{\sigma}}$ denote the independent displacement/rotation, enhanced strain and stress fields, with $\boldsymbol{u} = \boldsymbol{x} - \boldsymbol{X}$ the displacement vector and $\boldsymbol{\omega}$ the vector of rotational parameters of the shell middle surface. The strain energy W is a function of the total strains $\hat{\boldsymbol{\varepsilon}}$. Variation of the functional (62) with respect to the independent variables and introducing some orthogonality conditions in order to eliminate the independent stresses from the set of equations yields the weak form of the

boundary value problem

$$\delta\Pi = \int\limits_{(\Omega)} \delta\boldsymbol{\varepsilon}^T \partial_{\hat{\boldsymbol{\varepsilon}}} W \, dA - \int\limits_{(\Omega)} \delta\boldsymbol{u}^T \bar{\boldsymbol{p}} \, dA - \int\limits_{(\Gamma_\sigma)} \delta\boldsymbol{u}^T \bar{\boldsymbol{t}} \, ds = 0 \tag{63}$$

with $\delta\hat{\boldsymbol{\varepsilon}} = \delta\boldsymbol{\varepsilon} + \delta\tilde{\boldsymbol{\varepsilon}}$ and $\delta\boldsymbol{\varepsilon} = [\delta\varepsilon_{11}, \delta\varepsilon_{22}, 2\delta\varepsilon_{12}, \delta\kappa_{11}, \delta\kappa_{22}, 2\delta\kappa_{12}, \delta\gamma_1, \delta\gamma_2]^T$. Herein, the individual parts are computed by

$$\begin{aligned} \delta\varepsilon_{\alpha\beta} &= \frac{1}{2}(\delta\boldsymbol{x}_{,\alpha}\cdot\boldsymbol{x}_{,\beta} + \delta\boldsymbol{x}_{,\beta}\cdot\boldsymbol{x}_{,\alpha}), \\ \delta\kappa_{\alpha\beta} &= \frac{1}{2}(\delta\boldsymbol{x}_{,\alpha}\cdot\boldsymbol{d}_{,\beta} + \delta\boldsymbol{x}_{,\beta}\cdot\boldsymbol{d}_{,\alpha} + \delta\boldsymbol{d}_{,\alpha}\cdot\boldsymbol{x}_{,\beta} + \delta\boldsymbol{d}_{,\beta}\cdot\boldsymbol{x}_{,\alpha}), \\ \delta\gamma_\alpha &= \delta\boldsymbol{x}_{,\alpha}\cdot\boldsymbol{d} + \delta\boldsymbol{d}\cdot\boldsymbol{x}_{,\alpha}\ . \end{aligned} \tag{64}$$

For the sake of completeness, the local Euler-Lagrange equations associated with the variation of (62) can be obtained with integration by parts and standard arguments of variational calculus and yield the following equations in Ω and stress boundary conditions on Γ_σ:

$$\left.\begin{aligned} \tfrac{1}{j}(j\,\boldsymbol{n}^\alpha)_{,\alpha} + \bar{\boldsymbol{p}} = \boldsymbol{0}, \qquad & \tilde{\boldsymbol{\varepsilon}} = \boldsymbol{0} \\ \tfrac{1}{j}(j\,\boldsymbol{m}^\alpha)_{,\alpha} + \boldsymbol{x}_{,\alpha}\times\boldsymbol{n}_\alpha = \boldsymbol{0}, \qquad & \partial_{\boldsymbol{\varepsilon}} W - \tilde{\boldsymbol{\sigma}} = \boldsymbol{0} \end{aligned}\right\} \quad \text{in} \quad \Omega\,,$$

$$\left.\begin{aligned} j\,(\boldsymbol{n}^\alpha\,\nu_\alpha) - \bar{\boldsymbol{t}} = \boldsymbol{0}, \qquad & j\,(\boldsymbol{m}^\alpha\,\nu_\alpha) = \boldsymbol{0} \end{aligned}\right\} \quad \text{on} \quad \Gamma_\sigma\,. \tag{65}$$

Herein, we have $\boldsymbol{n}^\alpha = n^{\alpha\beta}\,\boldsymbol{x}_{,\beta} + q^\alpha\boldsymbol{d} := \tilde{n}^{\alpha\beta}\,\boldsymbol{x}_{,\beta} + \tilde{q}^\alpha\boldsymbol{d} + \tilde{m}^{\alpha\beta}\,\boldsymbol{d}_{,\beta}$ with membrane forces $\tilde{n}^{\alpha\beta} = \tilde{n}^{\beta\alpha}$, bending moments $\tilde{m}^{\alpha\beta} = \tilde{m}^{\beta\alpha}$ and shear forces $\tilde{q}^\alpha$ and $\boldsymbol{m}^\alpha := \boldsymbol{d}\times m^{\alpha\beta}\,\boldsymbol{x}_{,\beta}$ with $m^{\alpha\beta} = \tilde{m}^{\alpha\beta}$ and the components ν_α of the normal vector to the boundary. The effective stress resultants $\tilde{n}^{\alpha\beta}$ and $\tilde{q}^\alpha$ are related to the stress resultants $n^{\alpha\beta}$ and q^α by well-known relations, Green and Naghdi (1974). The geometric boundary conditions $\boldsymbol{u} - \bar{\boldsymbol{u}} = \boldsymbol{0}$ on Γ_u have to be fulfilled as constraints. In the following, the stress resultants obtained by partial derivatives of the strain energy function are denoted by $\boldsymbol{\sigma} := \partial_{\hat{\boldsymbol{\varepsilon}}} W$, whose components are arranged according to (61),

$$\boldsymbol{\sigma} = [\tilde{n}^{11}, \tilde{n}^{22}, \tilde{n}^{12}, \tilde{m}^{11}, \tilde{m}^{22}, \tilde{m}^{12}, \tilde{q}^1, \tilde{q}^2]^T\,. \tag{66}$$

The field variables are approximated by using the isoparametric concept and bi-linear ansatz functions for the position and director vectors. Then the weak form is linearized in order to get the stiffness matrix and residual vector, for details we refer to Balzani et al. (2008).

5.3 Interface to General 3D-Constitutive Laws

This section explains the interface of the shell element to general nonlinear three-dimensional constitutive laws as pointed out in Section 3 and provides the numerical integration of the stress resultants. As a starting point we consider the relation between the strains at a layer point with coordinate ξ^3 and the shell strains (59) in matrix notation $\bar{\boldsymbol{E}}_m = [E_{11}, E_{22}, E_{12}, E_{13}, E_{23}]^T$, which is rewritten by

$$\bar{\mathbf{E}}_m = \boldsymbol{A}\,\boldsymbol{\varepsilon} = \begin{bmatrix} 1 & 0 & 0 & \xi^3 & 0 & 0 & 0 & 0 \\ 0 & 1 & 0 & 0 & \xi^3 & 0 & 0 & 0 \\ 0 & 0 & 1 & 0 & 0 & \xi^3 & 0 & 0 \\ 0 & 0 & 0 & 0 & 0 & 0 & 1 & 0 \\ 0 & 0 & 0 & 0 & 0 & 0 & 0 & 1 \end{bmatrix} \begin{bmatrix} \varepsilon_{11} \\ \varepsilon_{22} \\ 2\varepsilon_{12} \\ \kappa_{11} \\ \kappa_{22} \\ 2\kappa_{12} \\ \gamma_1 \\ \gamma_2 \end{bmatrix} . \tag{67}$$

In this section we use $(\bullet)$ for tensorial quantities arranged in vectors or matrices, e.g. the second-order tensor $\mathbf{E}$ can be written as vector $\bar{\mathbf{E}}$. The kinematic shell model assumes inextensibility in thickness direction. Thus, the zero normal stress condition has to be enforced, which then yields the thickness strains, see Dvorkin et al. (1995) and Klinkel and Govindjee (2002). For this purpose we consider the stresses to be organized in a vector given by

$$\bar{\mathbf{S}} = \begin{bmatrix} \bar{\boldsymbol{S}}^m \\ S^{33} \end{bmatrix} . \tag{68}$$

Herein, $\bar{\mathbf{S}}^m = [S^{11}, S^{22}, S^{12}, S^{13}, S^{23}]^T$ are the Second Piola-Kirchhoff stresses, which are obtained by evaluating a general nonlinear three-dimensional constitutive law. In order to derive the vector of the stress resultants we insert (67) in the internal virtual work expression of the body and obtain

$$\boldsymbol{\sigma}^h = \int_{(-h/2)}^{(h/2)} \boldsymbol{A}^T \bar{\mathbf{S}}^m \, \bar{\mu} \, d\xi^3 \,, \tag{69}$$

where $\bar{\mu}$ denotes the determinant of the shifter tensor. The zero normal stress condition $S^{33}(E_{33}) = 0$ is iteratively enforced. For this purpose the increment of the Second Piola–Kirchhoff stress tensor is reformulated in matrix notation by

$$\mathrm{d}\bar{\mathbf{S}} = \begin{bmatrix} \mathrm{d}\bar{\mathbf{S}}^m \\ \mathrm{d}S^{33} \end{bmatrix} = \begin{bmatrix} \bar{\mathbb{C}}^{mm} & \bar{\mathbb{C}}^{m3} \\ \bar{\mathbb{C}}^{3m} & \bar{\mathbb{C}}^{33} \end{bmatrix} \begin{bmatrix} \mathrm{d}\bar{\mathbf{E}}_m \\ \mathrm{d}E_{33} \end{bmatrix} = \bar{\mathbb{C}}\,\mathrm{d}\bar{\mathbf{E}} \,, \tag{70}$$

where $\bar{\mathbb{C}} = \partial_{\bar{E}} \bar{\mathbf{S}}$ denotes the material tangent which is determined within a three–dimensional stress analysis at the considered point in shell space. The Taylor series of the zero normal stress condition is aborted after the linear term and set to zero. Then the normal stress condition reads

$$S^{33(i)} + \bar{\mathbb{C}}^{33(i)} \, \Delta E_{33}^{(i+1)} = 0 \quad \text{with} \quad \bar{\mathbb{C}}^{33(i)} = \frac{\mathrm{d}S^{33(i)}}{\mathrm{d}E_{33}^{(i)}} \tag{71}$$

and the solution yields the update formula

$$E_{33}^{(i+1)} = E_{33}^{(i)} - \frac{S^{33(i)}}{\bar{\mathbb{C}}^{33(i)}} \,, \tag{72}$$

where i denotes the iteration number. Thus, the nonlinear scalar equation $S^{33}(E_{33}) = 0$ is iteratively solved for the unknown thickness strains using Newtons scheme. One obtains the stress vector $\bar{\mathbf{S}}^m$ and the tangent matrix $\bar{\mathbb{C}}$ with submatrices according to (70). The algorithm provides an interface to arbitrary nonlinear three–dimensional material laws. It requires the computation of $\bar{\mathbf{S}}$ and $\bar{\mathbb{C}}$ which is a standard output of any nonlinear three–dimensional stress analysis.

5.4 Examples: Influence of Anisotropy

To provide numerical examples this section discusses two examples, where polyconvex anisotropic hyperelastic strain energy functions are used. For an illustration of the anisotropy effects the simulations of anisotropic shells are compared with the results of similar isotropic ones. Due to the fact that fiber reinforced shells often show a different behavior in warp and fill direction, a quadratic plate with two preferred directions characterized by different material properties is considered first. Second, a hyperbolic shell is taken into account, where the material is reinforced in one preferred direction. It is remarked that in all numerical calculations the solution for each load step is found after 4 to 6 Newton iterations for both, the isotropic and the anisotropic case.

Quadratic Plate with two Different Fiber Types This example considers a thin quadratic plate consisting of a typical membrane-like engineering material with a particular behavior in warp and fill direction. To analyze the influence of anisotropy we submit a follower load (perpendicular to the deformed mid-surface) and compare the solution of this plate with the results of an isotropic plate.

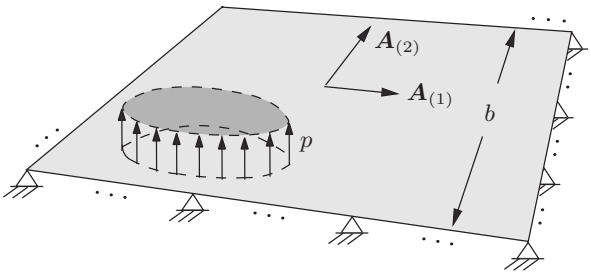

Figure 5: Boundary conditions of the thin quadratic plate and fiber directions $\boldsymbol{A}_{(1)} = (1 \quad 0 \quad 0)^T$ and $\boldsymbol{A}_{(2)} = (0 \quad 1 \quad 0)^T$.

The width and thickness of the quadratic plate are set to $b = 0.1$ m and 2.0 mm, respectively. The boundary conditions are shown in Fig. 5. For the description of the isotropic behavior we use the strain energy density

$$\psi_{iso} = c_1 \left(I_1 \, I_3^{-1/3} - 3 \right) + \epsilon_1 \left(I_3^{\epsilon_2} + I_3^{-\epsilon_2} - 2 \right) \tag{73}$$

and the energy associated with each fiber direction is represented by

$$\psi_{(a)}^{ti} = \alpha_1^{(a)} \left\langle K_3^{(a)} - 2 \right\rangle^{\alpha_2^{(a)}} . \tag{74}$$

Since different fiber properties are assumed for the warp and fill direction also different material parameters for the two directions are taken into account. Thus, we set $n_f = 2$ and the complete energy reads

$$\psi = \psi_{iso} + \alpha_1^{(1)} \left\langle K_3^{(1)} - 2 \right\rangle^{\alpha_2^{(1)}} + \alpha_1^{(2)} \left\langle K_3^{(2)} - 2 \right\rangle^{\alpha_2^{(2)}} . \tag{75}$$

The warp direction is aligned in x-direction, i.e. $\mathbf{A}_{(1)} = (1 \quad 0 \quad 0)^T$, and the fill direction is oriented in y-direction, i.e. $\mathbf{A}_{(2)} = (0 \quad 1 \quad 0)^T$. The

parameters are set to

$$\begin{aligned} c_1 &= 1.0\ \mathrm{kN/mm^2}, \\ \epsilon_1 &= 100.0\ \mathrm{kN/mm^2}, \quad \epsilon_2 = 5.0, \\ \alpha_1^{(1)} &= 98.0\ \mathrm{kN/mm^2}, \quad \alpha_2^{(1)} = 3.0\,, \\ \alpha_1^{(2)} &= 140.0\ \mathrm{kN/mm^2}, \quad \alpha_2^{(2)} = 2.3\,. \end{aligned} \tag{76}$$

Then we obtain the material behavior as depicted in Fig. 6, where the force-strain response of the considered material is illustrated for a biaxial tension test and a uniaxial tension/compression test in x- and y-direction.

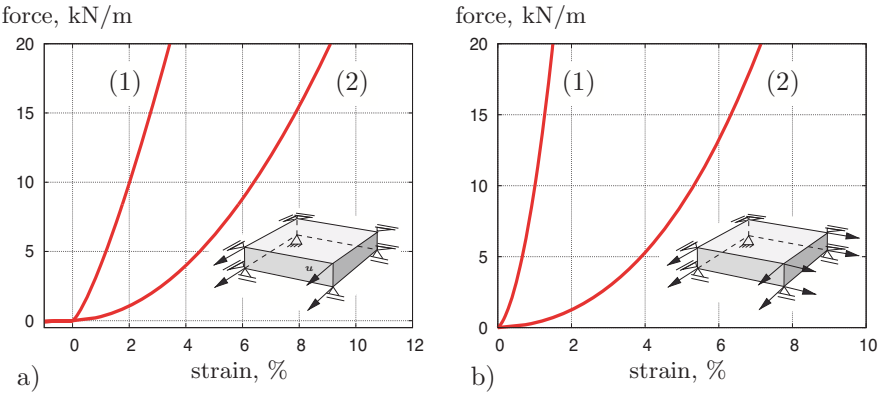

Figure 6: Force-strain response of a) uniaxial tension/compression test and b) biaxial tension test; (1) warp- and (2) fill-direction.

For the numerical analysis we increase the load parameter until we obtain a maximum vertical displacement of approximately $u_3 = 130.0$ mm for the isotropic and the anisotropic plate. We investigate the discretization of the plate with 1600 four-node shell elements. In Fig. 7 the distribution of n^{11} and n^{22} is depicted. For the isotropic case we notice that the distribution of n^{11} is identical to the rotated distribution of n^{22} by 90°, which directly results from isotropy. In the anisotropic case we observe, due to the differing stiffness in warp and fill direction, a significantly different response concerning the quantitative normal forces n^{11} and n^{22}, which becomes obvious when comparing Fig. 7b with 7d.

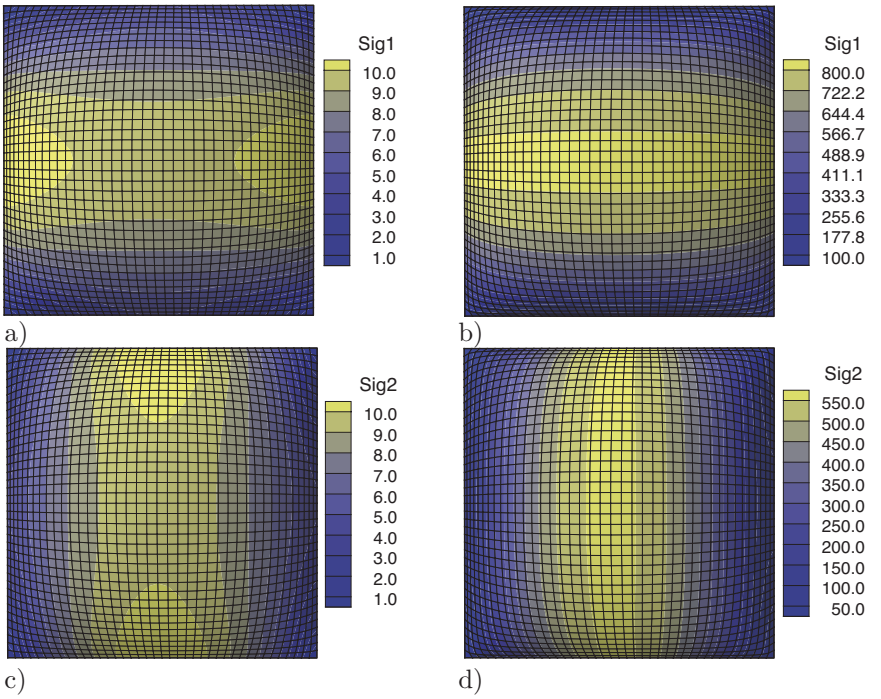

Figure 7: Normal force in x-direction n^{11} and in y-direction n^{22} for the a,c) isotropic and b,d) anisotropic plate, respectively.

Hyperbolic Shell Subjected to Locally Distributed Loads In this section we investigate a hyperbolic shell, which is subjected to four pairs of locally distributed vertical loads, cp. Başar and Ding (1997) or Başar and Grytz (2004). In Fig. 8 the boundary value problem and the discretization with 3200 four-node shell-elements are depicted.

The height is defined to be $H = 12.0$ m and for the thickness of the shell 0.05 m are chosen. The radius of the hyperbolic shell is computed as a function of the z-coordinate, i.e.

$$R(z) = R_T \sqrt{1 + \left(\frac{z - \frac{H}{2}}{2.0} \right)^2} \,, \tag{77}$$

wherein the minimum radius is set to $R_T = 3.0$ m. For an illustration of the

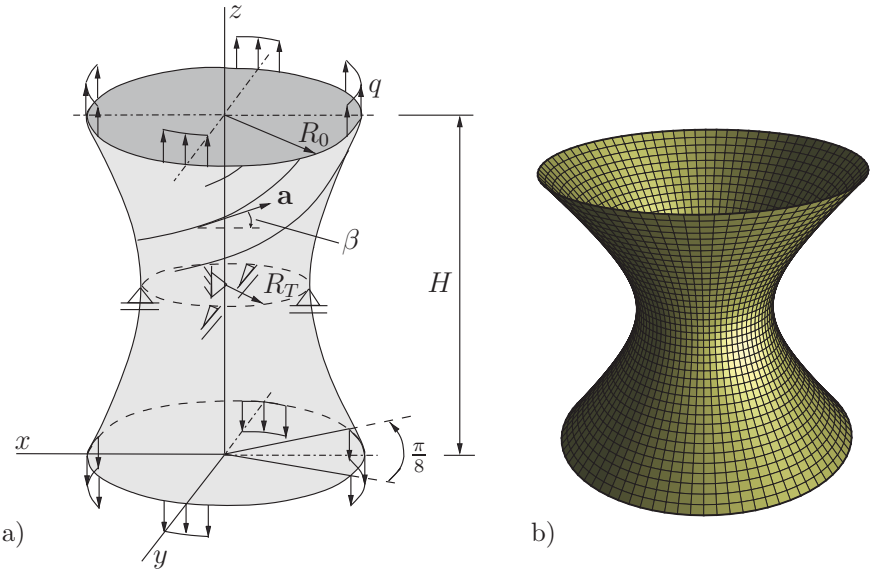

Figure 8: Hyperbolic shell: a) schematic sketch of the system with boundary conditions and b) discretization with 3200 four-node shell elements.

anisotropy we compare the simulation of an i) isotropic and a ii) transversely isotropic shell, where locally distributed loads at the top and bottom of the hyperboloid extend the structure in z-direction. For the isotropic and the transversely isotropic energy the same functions as for the plate in the previous section are used. Since for the anisotropic shell only one fiber direction $\mathbf{A}$ is taken into account, which is aligned as a helix around the hyperbolic shell with $\beta = 45.0°$, cp. Fig. 8a, we set $n_f = 1$ and the complete energy reads

$$\psi = \psi_{iso} + \alpha_1 \langle K_3 - 2 \rangle^{\alpha_2} \ . \tag{78}$$

The material parameters are set to

$$\begin{array}{rclrclrcl} c_1 & = & 100.0\,\mathrm{kN/m^2}\,, & \epsilon_1 & = & 2000.0\,\mathrm{kN/m^2}\,, & \epsilon_2 & = & 10.0, \\ \alpha_1 & = & 5000.0\,\mathrm{kN/m^2}\,, & \alpha_2 & = & 2.3\,. & & & \end{array} \tag{79}$$

In order to be able to qualitatively compare the transversely isotropic with the isotropic shell we apply concentrated loads in each structure such that a vertical displacement of approximately $u_3 = 2.0$ m is reached. When comparing the deformed structure of both shells as depicted in Fig. 9, we

observe a significant difference. The deformed isotropic shell is symmetric with respect to the global coordinate axis, while the transversely isotropic shell is twisted although only a symmetric force in z-direction is applied.

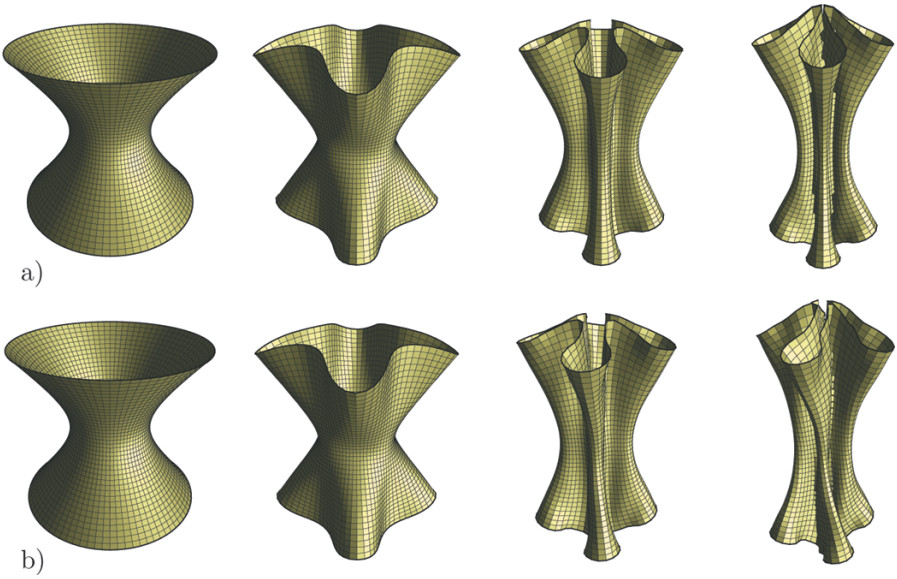

Figure 9: Different deformation states (from the left to the right: from the undeformed to the completely deformed state) for the a) isotropic and b) transversely isotropic shell.

The reason is obviously the stiff fibers providing a strong reinforcement in the diagonal direction around the hyperbolic shell. The exponential character of the transversely isotropic energy function is shown by the fact that the anisotropic shell behaves nearly isotropic in the beginning, too, see Figs. $9b_{1,2}$, where no twisting is observed. But then for larger deformations the anisotropic influence increases until the twist becomes significant in Fig. $9b_4$.

6 Conclusion

In this contribution it was shown that the polyconvexity condition seems to be a suitable condition for the construction of energy functions, also with respect to engineering applications. By satisfying this condition the

existence of minimizers has been guaranteed as well as material stability. In the framework of polyconvexity the stress-free reference configuration is in general not able to be satisfied automatically. Thus, a simple construction principle was proposed based on the property that external convex and monotonically increasing functions of internal polyconvex functions are again polyconvex and a variety of transversely isotropic energy functions was constructed. These functions were discussed with respect to the description of soft biological tissues and their applicability has been illustrated by the comparison with experiments showing a good aggreement. In addition to this, thin shell problems were analyzed at finite strains. For the incorporation of the polyconvex strain energies in the considered shell formulation an interface for a general three-dimensional constitutive model was described. Several numerical examples were investigated where an isotropic plate and shell was compared with anisotropic ones. When comparing the isotropic and anisotropic cases, significant differences of the deformation and also of the distribution of some representative stress-resultants were observed.

Acknowledgements The authors greatly appreciate Prof. G.A. Holzapfel for the experimental data of arterial walls, Prof. F. Gruttmann for a fruitful cooperation (Balzani, Gruttmann & Schröder (2008)), and S. Brinkhues for the parameter adjustment. In addition, the financial support from the DFG (research grant SCHR 570/7-2) is greatfully acknowledged.

Bibliography

Y. Başar and Y. Ding. Shear deformation models for large-strain shell analysis. *International Journal of Solids and Structures*, 34:1687–1708, 1997.

Y. Başar and R. Grytz. Incompressibility at large strains and finite-element implementation. *Acta Mechanica*, 168:75–101, 2004.

J. M. Ball. Constitutive equalities and existence theorems in elasticity. In R. J. Knops, editor, *Symposium on Non-Well Posed Problems and Logarithmic Convexity*, volume 316. Springer-Lecture Notes in Math., 1977a.

J.M. Ball. Convexity conditions and existence theorems in non-linear elasticity. *Archive for Rational Mechanics and Analysis*, 63:337–403, 1977b.

D. Balzani. *Polyconvex anisotropic energies and modeling of damage applied to arterial walls*. Phd-thesis, University Duisburg-Essen, Verlag Glückauf Essen, 2006.

D. Balzani, P. Neff, J. Schröder, and G.A. Holzapfel. A polyconvex framework for soft biological tissues. Adjustment to experimental data. *International Journal of Solids and Structures*, 43(20):6052–6070, 2006.

D. Balzani, F. Gruttmann, and J. Schröder. Analysis of thin shells using anisotropic polyconvex energy densities. *Computer Methods in Applied Mechanics and Engineering*, 197:1015–1032, 2008.

P. Betsch, F. Gruttmann, and E. Stein. A 4-node finite shell element for the implementation of general hyperelastic 3D-elasticity at finite strains. *Computer Methods in Applied Mechanics and Engineering*, 130:57–79, 1996.

J. Betten. Formulation of anisotropic constitutive equations. In J.P. Boehler, editor, *Applications of tensor functions in solid mechanics*, volume 292 of *Courses and Lectures of CISM*. Springer, 1987.

J.P. Boehler. Introduction to the invariant formulation of anisotropic constitutive equations. In J.P. Boehler, editor, *Applications of tensor functions in solid mechanics*, number 292 in Courses and Lectures of CISM, pages 13–30. Springer, 1987.

B.D. Coleman and W. Noll. On the thermostatics of continuous media. *Archive of Rational Mechanics and Analysis*, 4:97–128, 1959.

B. Dacorogna. Direct methods in the calculus of variations. *Applied Mathematical Science*, 78, 1989.

T.C. Doyle and J.L. Ericksen. Nonlinear elasticity. In H.L. Dryden and Th. von Kármán, editors, *Advances in Applied Mechanics IV*. Academic Press, New York, 1956.

E. Dvorkin, D. Pantuso, and E. Repetto. A formulation of the mitc4 shell element for finite strain elasto-plastic analysis. 125:17–40, 1995.

A. Ehret and M. Itskov. A polyconvex hyperelastic model for fiber-reinforced materials in application to soft tisues. *Journal of Material Science*, 42: 8853–9963, 2007.

J.L. Ericksen and R.S. Rivlin. Large elastic deformations of homogeneous anisotropic materials. *Journal of Rational Mechanics and Analysis*, 3: 281–301, 1957.

T. Gasser, R. Ogden, and G.A. Holzapfel. Hyperelastic modelling of arterial layers with distributed collagen fibre orientations. *Journal of the Royal Society Interface*, 3:15–35, 2006.

A.E. Green and P.M. Naghdi. On the derivation of shell theories by direct approach. *Journal of Applied Mechanics*, 41:173–176, 1974.

S. Hartmann and P. Neff. Existence theory for a modified polyconvex hyperelastic relation of generalized polynomial-type in the case of nearly-incompressibility. *International Journal of Solids and Structures*, 40: 2767–2791, 2003.

G. A. Holzapfel. Determination of material models for arterial walls from uniaxial extension tests and histological structure. *Journal of Theoretical Biology*, 238(2):290–302, 2006.

G. A. Holzapfel, Th.C. Gasser, and R.W. Ogden. A new constitutive framework for arterial wall mechanics and a comparative study of material models. *Journal of Elasticity*, 61:1–48, 2000.

G.A. Holzapfel, T.C. Gasser, and R.W. Ogden. Comparison of a multi-layer structural model for arterial walls with a fung-type model, and issues of material stability. *Journal of Biomechanical Engineering*, 126:264–275, 2004a.

G.A. Holzapfel, G. Sommer, and P. Regitnig. Anisotropic mechanical properties of tissue components in human atherosclerotic plaques. *Journal of Biomechanical Engineering*, 126:657–665, 2004b.

M. Itskov and A. Aksel. A class of orthotropic and transversely isotropic hyperelastic constitutive models based on a polyconvex strain energy function. *International Journal of Solids and Structures*, 41(14):3833–3848, 2004.

S. Klinkel and S. Govindjee. Using finite strain 3D-material models in beam and shell elements. *Engineering Computations*, 19(8):902–921, 2002.

B. Markert, W. Ehlers, and N. Karajan. A general polyconvex strain-energy function for fiber-reinforced materials. *Proceedings of Applied Mathematics and Mechanics*, 5:245–246, 2005.

J. Merodio and P. Neff. A note on tensile instabilities and loss of ellipticity for a fiber-reinforced nonlinearly elastic solid. *Archive of Applied Mechanics*, 58:293–303, 2006.

C.B. Morrey. Quasi-connvexity and the lower semicontinuity of multiple integrals. *Pacific Journal of Mathematics*, 2:25–53, 1952.

P. Neff. *Mathematische Analyse multiplikativer Viskoplastizität.* Shaker verlag, isbn:3-8265-7560-1, Fachbereich Mathematik, Technische Universität Darmstadt, 2000.

M.R. Roach and A.C. Burton. The reason for the shape of the distensibility curves of arteries. 35:681–690, 1957.

M. Rüter and E. Stein. Analysis, finite element computation and error estimation in transversely isotropic nearly incompressible finite elasticity. *Computer Methods in Applied Mechanics and Engineering*, 190:519–541, 2000.

J. Schröder and N. Neff. On the construction of polyconvex anisotropic free energy functions. In C. Miehe, editor, *Proceedings of the IUTAM Symposium on Computational Mechanics of Solid Materials at Large Strains*, pages 171–180, Dordrecht, 2001. Kluwer Adcademic Publishers.

J. Schröder and P. Neff. Application of polyconvex anisotropic free energies to soft tissues. In H.A. Mang, F.G. Rammerstorfer, and J. Eberhardsteiner, editors, *Proccedings of the Fifth World Congress on Computational Mechanics (WCCM V) in Vienna, Austria,*, 2002.

J. Schröder and P. Neff. Invariant formulation of hyperelastic transverse isotropy based on polyconvex free energy functions. *International Journal of Solids and Structures*, 40:401–445, 2003.

J. Schröder, P. Neff, and D. Balzani. A variational approach for materially stable anisotropic hyperelasticity. *International Journal of Solids and Structures*, 42(15):4352–4371, 2005.

J. Schröder, P. Neff, and V. Ebbing. Anisotropic polyconvex energies on the basis of crystallographic motivated structural tensors. *Journal of the Mechanics and Physics of Solids*, 56(12):3486–3506, 2008.

C. A. J. Schulze-Bauer, P. Regitnig, and G. A. Holzapfel. Mechanics of the human femoral adventitia including the high-pressure response. *American Journal of Physiology - Heart and Circulatory Physiology*, 282: H2427–H2440, 2002.

J.C. Simo and F. Armero. Geometrically non-linear enhanced strain mixed methods and the method of incompatible modes. *International Journal for Numerical Methods in Engineering*, 33:1413–1449, 1992.

J.C. Simo and M.S. Rifai. A class of mixed assumed strain methods and the method of incompatible modes. *International Journal for Numerical Methods in Engineering*, 29:1595–1638, 1990.

A. J. M. Spencer. *Continuum Physics Vol. 1*, chapter Theory of Invariants, pages 239–353. Academic Press, New York, 1971.

J.A. Weiss, B.N. Maker, and S. Govindjee. Finite element implementation of incompressible, transversely isotropic hyperelasticity. *Computer Methods in Applied Mechanics and Engineering*, 135:107–128, 1996.

Q.S. Zheng and A.J.M. Spencer. Tensors which characterize anisotropies. *International Journal of Engineering Science*, 31(5):679–693, 1993.

Appendix

Isotropic functions using $I_1 = \mathrm{tr}[\boldsymbol{C}]$, $I_2 = \mathrm{tr}[\mathrm{Cof}[\boldsymbol{C}]]$, $I_3 = \det[\boldsymbol{C}]$		
Polyconvex function	Restrictions	Stress-free r.c.
[1.] $\alpha_1 I_1^{\alpha_2}$	$\alpha_1 > 0,\ \alpha_2 \geq 1$	no
[1.] $\alpha_1 I_2^{\alpha_2}$	$\alpha_1 > 0,\ \alpha_2 \geq 1$	no
[1.] $\alpha_1 \dfrac{I_1}{I_3^{1/3}}$	$\alpha_1 > 0$	no
[1.] $\alpha_1 \dfrac{I_1^2}{I_3^{1/3}}$	$\alpha_1 > 0$	no
[1.] $\alpha_1 \dfrac{I_2}{I_3^{1/3}}$	$\alpha_1 > 0$	no
[1.] $\alpha_1 \dfrac{I_2^2}{I_3^{1/3}}$	$\alpha_1 > 0$	no
[1.] $\alpha_1 I_3^{\alpha_2}$	$\alpha_1 > 0,\ \ \alpha_2 \geq 1,\ \ I_3 > 0$	no
[1.] $\alpha_1 \dfrac{1}{I_3}$	$\alpha_1 > 0$	no
[1.] $-\alpha_1 \ln(I_3)$	$\alpha_1 > 0$	no
[1.] $-\alpha_1 \ln(\sqrt{I_3})$	$\alpha_1 > 0$	no
[1.] $\alpha_1 \left(I_3 + \dfrac{1}{I_3}\right)$	$\alpha_1 > 0$	yes
[1.] $\alpha_1 \left(I_3 - 1\right)^2$	$\alpha_1 > 0$	yes
[1.] $\alpha_1 \left(I_3^{\alpha_2} + \dfrac{1}{I_3^{\alpha_2}} - 2\right)^{\alpha_3}$	$\alpha_1 > 0,\ \ \alpha_2 \geq \alpha_3 \geq 1$	yes
[1.] $\alpha_1 \left(\sqrt{I_3} - 1\right)^{\alpha_2}$	$\alpha_1 > 0,\ \ \alpha_2 \geq 1$	yes
[1.] $\alpha_1 \left[I_3 - \ln(I_3)\right]$	$\alpha_1 > 0$	yes

[1.] cp. e.g. Hartmann and Neff (2003), Schröder and Neff (2003)

Isotropic functions (continued)

Polyconvex function	Restrictions	Stress-free r.c.
[1.] $\alpha_1 \left\{ I_3 - \ln(I_3) + [\ln(I_3)]^2 \right\}$	$\alpha_1 > 0$	yes
[1.] $\alpha_1 \left(\frac{I_1^{\alpha_2}}{I_3^{\alpha_2/3}} - 3^{\alpha_2} \right)^{\alpha_3}$	$\alpha_1 > 0,\ \alpha_2 \geq 1\ \alpha_3 \geq 1$	yes
[1.] $\alpha_1 \left(\frac{I_2^{3\alpha_2/2}}{I_3^{\alpha_2}} - (3\sqrt{3})^{\alpha_2} \right)^{\alpha_3}$	$\alpha_1 > 0,\ \alpha_2 \geq 1\ \alpha_3 \geq 1$	yes
[1.] $\alpha_1 \left\{ \exp\left[\left(\frac{I_1^{\alpha_2}}{I_3^{\alpha_2/3}} - 3^{\alpha_2} \right)^{\alpha_3} \right] - 1 \right\}$	$\alpha_1 > 0,\ \alpha_2 \geq 1,\ \alpha_3 \geq 1$	yes
[1.] $\alpha_1 \left\{ \exp\left[\left(\frac{I_2^{3\alpha_2/2}}{I_3^{\alpha_2}} - 3(\sqrt{3})^{\alpha_2} \right)^{\alpha_3} \right] - 1 \right\}$	$\alpha_1 > 0,\ \alpha_2 \geq 1,\ \alpha_3 \geq 1$	yes
[2.] $\alpha_1 \left(\frac{I_1}{I_3^{1/3}} - 3 \right)$	$\alpha_1 > 0$	yes
[3.] $\alpha_1 \left(\frac{I_2}{I_3^{1/3}} - 3 \right)$	$\alpha_1 > 0$	no

[1.] cp. e.g. Hartmann and Neff (2003), Schröder and Neff (2003)
[2.] cp. e.g. Holzapfel et al. (2000) or Schröder et al. (2005)
[3.] cp. e.g. Schröder and Neff (2001), Schröder and Neff (2002) or Schröder et al. (2005)

Transversely isotropic functions using $I_1 = \mathrm{tr}[\boldsymbol{C}]$, $I_2 = \mathrm{tr}[\mathrm{Cof}[\boldsymbol{C}]]$, $I_3 = \det[\boldsymbol{C}]$,

$J_4 = \mathrm{tr}[\boldsymbol{C}\boldsymbol{M}]$, $J_5 = \mathrm{tr}[\mathrm{Cof}[\boldsymbol{C}]\boldsymbol{M}]$, $K_1 = J_5 - I_1\,J_4 + I_2$, $K_2 = I_1 - J_4$, $K_3 = I_1\,J_4 - J_5$:

Polyconvex function	Restrictions	Stress-free r.c.
[1.] $\alpha_1\, J_4^{\alpha_2}$	$\alpha_1 > 0,\ \alpha_2 \geq 1$	no
[1.] $\alpha_1\, \dfrac{J_4^{\alpha_2}}{I_3^{1/3}}$	$\alpha_1 > 0,\ \alpha_2 \geq 1$	no
[1.] $\alpha_1\, K_1^{\alpha_2}$	$\alpha_1 > 0,\ \alpha_2 \geq 1$	no
[1.] $\alpha_1\, \dfrac{K_1^{\alpha_2}}{I_3^{1/3}}$	$\alpha_1 > 0,\ \alpha_2 \geq 1$	no
[1.] $\alpha_1\, \dfrac{K_1^2}{I_3^{2/3}}$	$\alpha_1 > 0$	no
[1.] $\alpha_1\, K_2^{\alpha_2}$	$\alpha_1 > 0,\ \alpha_2 \geq 1$	no
[1.] $\alpha_1\, \dfrac{K_2^{\alpha_2}}{I_3^{1/3}}$	$\alpha_1 > 0,\ \alpha_2 \geq 1$	no
[1.] $\alpha_1\, \dfrac{K_2^2}{I_3^{2/3}}$	$\alpha_1 > 0$	no
[1.] $\alpha_1\, K_3^{\alpha_2}$	$\alpha_1 > 0,\ \alpha_2 \geq 1$	no
[1.] $\alpha_1\, \dfrac{K_3^{\alpha_2}}{I_3^{1/3}}$	$\alpha_1 > 0,\ \alpha_2 \geq 1$	no
[1.] $\alpha_1\, \big(I_1^2 + J_4\, I_1\big)$	$\alpha_1 > 0$	no
[1.] $\alpha_1\, \big(2I_1^2 - K_2\, I_1\big)$	$\alpha_1 > 0$	no
[1.] $\alpha_1\, \big(I_2^2 + K_2\, I_2\big)$	$\alpha_1 > 0$	no
[1.] $\alpha_1\, \big(2I_2^2 + K_3\, I_2\big)$	$\alpha_1 > 0$	no
[1.] $\alpha_1\, (\alpha_2\, I_1 - \alpha_3\, J_4)$	$\alpha_1 > 0,\ \alpha_2 \geq \alpha_3 > 0$	no
[1.] $\alpha_1\, (\alpha_2\, I_2 - \alpha_3\, K_1)$	$\alpha_1 > 0,\ \alpha_2 \geq \alpha_3 > 0$	no

[1.] see Schröder and Neff (2003)

Transversely isotropic functions (continued), power functions

Polyconvex function	Restrictions	Str.-fr. r.c.
[1.)] $\alpha_1 \, (J_4^{\alpha_3} - 1)^{\alpha_2}$	$\alpha_1 > 0,\ \alpha_2 \geq 1,\ \alpha_3 \geq 1,\ \ J_4 \geq 1$	yes
[1.)] $\alpha_1 \left(\dfrac{J_4^{\alpha_3}}{I_3^{1/3}} - 1 \right)^{\alpha_2}$	$\alpha_1 > 0,\ \alpha_2 \geq 1,\ \alpha_3 \geq 1,\ \ \dfrac{J_4^{\alpha_3}}{I_3^{1/3}} \geq 1$	yes
[1.)] $\alpha_1 \, (K_1^{\alpha_3} - 1)^{\alpha_2}$	$\alpha_1 > 0,\ \alpha_2 \geq 1,\ \alpha_3 \geq 1,\ \ K_1 \geq 1$	yes
[1.)] $\alpha_1 \left(\dfrac{K_1^{\alpha_3}}{I_3^{1/3}} - 1 \right)^{\alpha_2}$	$\alpha_1 > 0,\ \alpha_2 \geq 1,\ \alpha_3 \geq 1,\ \ \dfrac{K_1^{\alpha_3}}{I_3^{1/3}} \geq 1$	yes
[1.)] $\alpha_1 \left(\dfrac{K_1^2}{I_3^{2/3}} - 1 \right)^{\alpha_2}$	$\alpha_1 > 0,\ \alpha_2 \geq 1,\ \ \dfrac{K_1^2}{I_3^{2/3}} \geq 1$	yes
[1.)] $\alpha_1 \, (K_2^{\alpha_3} - 2^{\alpha_3})^{\alpha_2}$	$\alpha_1 > 0,\ \alpha_2 \geq 1,\ \alpha_3 \geq 1,\ \ K_2 \geq 2$	yes
[1.)] $\alpha_1 \left(\dfrac{K_2^{\alpha_3}}{I_3^{1/3}} - 2^{\alpha_3} \right)^{\alpha_2}$	$\alpha_1 > 0,\ \alpha_2 \geq 1,\ \alpha_3 \geq 1,\ \ \dfrac{K_2^{\alpha_3}}{I_3^{1/3}} \geq 2^{\alpha_3}$	yes
[1.)] $\alpha_1 \left(\dfrac{K_2^2}{I_3^{2/3}} - 4 \right)^{\alpha_2}$	$\alpha_1 > 0,\ \alpha_2 \geq 1,\ \ \dfrac{K_2^2}{I_3^{2/3}} \geq 4$	yes
[1.)] $\alpha_1 \, (K_3^{\alpha_3} - 2^{\alpha_3})^{\alpha_2}$	$\alpha_1 > 0,\ \alpha_2 \geq 1,\ \alpha_3 \geq 1,\ \ K_3 \geq 2$	yes
[1.)] $\alpha_1 \left(\dfrac{K_3^{\alpha_3}}{I_3^{1/3}} - 2^{\alpha_3} \right)^{\alpha_2}$	$\alpha_1 > 0,\ \alpha_2 \geq 1,\ \alpha_3 \geq 1,\ \ \dfrac{K_3^{\alpha_3}}{I_3^{1/3}} \geq 2^{\alpha_3}$	yes

[1.)] cp. Balzani et al. (2006), Balzani (2006). Please note that continuous tangent moduli are obtained for $\alpha_2 > 2$.

Transversely isotropic functions (continued), hyperbolic cosine

Polyconvex function	Restrictions	Stress-free r.c.
[1.)] $\alpha_1 \left[\cosh\left(J_4^{\alpha_2} - 1\right) - 1\right]$	$\alpha_1 > 0,\ \alpha_2 \geq 1,\ \ J_4 \geq 1$	yes
[1.)] $\alpha_1 \left[\cosh\left(\dfrac{J_4^{\alpha_2}}{I_3^{1/3}} - 1\right) - 1\right]$	$\alpha_1 > 0,\ \alpha_2 \geq 1,\ \ \dfrac{J_4^{\alpha_2}}{I_3^{1/3}} \geq 1$	yes
[1.)] $\alpha_1 \left[\cosh\left(K_1^{\alpha_2} - 1\right) - 1\right]$	$\alpha_1 > 0,\ \alpha_2 \geq 1,\ \ K_1 \geq 1$	yes
[1.)] $\alpha_1 \left[\cosh\left(\dfrac{K_1^{\alpha_2}}{I_3^{1/3}} - 1\right) - 1\right]$	$\alpha_1 > 0,\ \alpha_2 \geq 1,\ \ \dfrac{K_1^{\alpha_2}}{I_3^{1/3}} \geq 1$	yes
[1.)] $\alpha_1 \left[\cosh\left(\dfrac{K_1^{2}}{I_3^{2/3}} - 1\right) - 1\right]$	$\alpha_1 > 0,\ \ \dfrac{K_1^{2}}{I_3^{2/3}} \geq 1$	yes
[1.)] $\alpha_1 \left[\cosh\left(K_2^{\alpha_2} - 2^{\alpha_2}\right) - 1\right]$	$\alpha_1 > 0,\ \alpha_2 \geq 1,\ \ K_2 \geq 2$	yes
[1.)] $\alpha_1 \left[\cosh\left(\dfrac{K_2^{\alpha_2}}{I_3^{1/3}} - 2^{\alpha_2}\right) - 1\right]$	$\alpha_1 > 0,\ \alpha_2 \geq 1,\ \ \dfrac{K_2^{\alpha_2}}{I_3^{1/3}} \geq 2^{\alpha_2}$	yes
[1.)] $\alpha_1 \left[\cosh\left(\dfrac{K_2^{2}}{I_3^{2/3}} - 4\right) - 1\right]$	$\alpha_1 > 0,\ \ \dfrac{K_2^{2}}{I_3^{2/3}} \geq 4$	yes
[1.)] $\alpha_1 \left[\cosh\left(K_3^{\alpha_2} - 2^{\alpha_2}\right) - 1\right]$	$\alpha_1 > 0,\ \alpha_2 \geq 1,\ \ K_3^{\alpha_2} \geq 2$	yes
[1.)] $\alpha_1 \left[\cosh\left(\dfrac{K_3^{\alpha_2}}{I_3^{1/3}} - 2^{\alpha_2}\right) - 1\right]$	$\alpha_1 > 0,\ \alpha_2 \geq 1,\ \ \dfrac{K_3^{\alpha_2}}{I_3^{1/3}} \geq 2^{\alpha_2}$	yes

[1.)] cp. Balzani (2006)

Transversely isotropic functions (continued), exponential functions

Polyconvex function	Restrictions	Str.-fr. r.c.
[1.] $\frac{\alpha_1}{2\alpha_2}\left\{\exp\left[\alpha_2\left(J_4^{\alpha_3}-1\right)^2\right]-1\right\}$	$\alpha_1>0,\ \alpha_2>0,\ \alpha_3\geq 1,\ \ J_4^{\alpha_3}\geq 1$	yes
[1.] $\frac{\alpha_1}{2\alpha_2}\left\{\exp\left[\alpha_2\left(\frac{J_4^{\alpha_3}}{I_3^{1/3}}-1\right)^2\right]-1\right\}$	$\alpha_1>0,\ \alpha_2>0,\ \alpha_3\geq 1,\ \ \frac{J_4^{\alpha_3}}{I_3^{1/3}}\geq 1$	yes
[1.] $\frac{\alpha_1}{2\alpha_2}\left\{\exp\left[\alpha_2\left(K_1^{\alpha_3}-1\right)^2\right]-1\right\}$	$\alpha_1>0,\ \alpha_2>0,\ \alpha_3\geq 1,\ \ K_1^{\alpha_2}\geq 1$	yes
[1.] $\frac{\alpha_1}{2\alpha_2}\left\{\exp\left[\alpha_2\left(\frac{K_1^{\alpha_3}}{I_3^{1/3}}-1\right)^2\right]-1\right\}$	$\alpha_1>0,\ \alpha_2>0,\ \alpha_3\geq 1,\ \ \frac{K_1^{\alpha_2}}{I_3^{1/3}}\geq 1$	yes
[1.] $\frac{\alpha_1}{2\alpha_2}\left\{\exp\left[\alpha_2\left(\frac{K_1^2}{I_3^{2/3}}-1\right)^2\right]-1\right\}$	$\alpha_1>0,\ \alpha_2>0,\ \ \frac{K_1^2}{I_3^{2/3}}\geq 1$	yes
[1.] $\frac{\alpha_1}{2\alpha_2}\left\{\exp\left[\alpha_2\left(K_2^{\alpha_3}-2^{\alpha_3}\right)^2\right]-1\right\}$	$\alpha_1>0,\ \alpha_2>0,\ \alpha_3>1,\ \ K_2\geq 2$	yes
[1.] $\frac{\alpha_1}{2\alpha_2}\left\{\exp\left[\alpha_2\left(\frac{K_2^{\alpha_3}}{I_3^{1/3}}-2^{\alpha_3}\right)^2\right]-1\right\}$	$\alpha_1>0,\ \alpha_2>0,\ \alpha_3\geq 1,\ \ \frac{K_2^{\alpha_2}}{I_3^{1/3}}\geq 2^{\alpha_3}$	yes
[1.] $\frac{\alpha_1}{2\alpha_2}\left\{\exp\left[\alpha_2\left(\frac{K_2^2}{I_3^{2/3}}-4\right)^2\right]-1\right\}$	$\alpha_1>0,\ \alpha_2>0,\ \ \frac{K_2^2}{I_3^{2/3}}\geq 4$	yes
[1.] $\frac{\alpha_1}{2\alpha_2}\left\{\exp\left[\alpha_2\left(K_3^{\alpha_3}-2^{\alpha_3}\right)^2\right]-1\right\}$	$\alpha_1>0,\ \alpha_2>0,\ \alpha_3\geq 1,\ \ K_3\geq 2$	yes
[1.] $\frac{\alpha_1}{2\alpha_2}\left\{\exp\left[\alpha_2\left(\frac{K_3^{\alpha_3}}{I_3^{1/3}}-2^{\alpha_3}\right)^2\right]-1\right\}$	$\alpha_1>0,\ \alpha_2>0,\ \alpha_3\geq 1,\ \ \frac{K_3^{\alpha_3}}{I_3^{1/3}}\geq 2^{\alpha_3}$	yes

[1.] cp. Balzani et al. (2006), Balzani (2006)

Transversely isotropic functions, special models

Polyconvex function	Restrictions	Str.-fr. r.c.
[1.] $\frac{\alpha_1}{2\alpha_2}\left\{\exp\left[\alpha_2\left(\frac{J_4}{I_3^{1/3}}-1\right)^2\right]-1\right\}$	$\alpha_1>0,\ \alpha_2>0,\ \alpha_3\geq 1,\ \ \frac{J_4}{I_3^{1/3}}\geq 1$	yes
[2.] $\frac{1}{4}\sum_r \mu_r\left[\frac{1}{\alpha_r}\left(\left(\sum_i w_i^{(r)}\hat{I}_i\right)^{\alpha_r}-1\right)+\frac{1}{\beta_r}\left(\left(\sum_i w_i^{(r)}\hat{J}_i\right)^{\beta_r}-1\right)+\frac{1}{\gamma_r}\left(I_3^{-\gamma_r}-1\right)\right]$	$\mu_r\geq 0,\ \alpha_r\geq 1,\ \beta_r\geq 1,\ \gamma_r\geq -\frac{1}{2}$	yes
with $\hat{I}_i=\mathrm{tr}[\boldsymbol{C}\boldsymbol{L}_i],\ \hat{J}_i=\mathrm{tr}[\mathrm{Cof}[\boldsymbol{C}]\boldsymbol{L}_i]$	$\sum_i w_i^{(r)}=1,\ r=1,2,...$	
and $\boldsymbol{L}_1=\boldsymbol{M},\ \boldsymbol{L}_2=\frac{1}{2}(\mathbf{1}-\boldsymbol{M})$		
[3.] $\sum_m\left(\frac{\tilde{\mu}_m}{\gamma_m}\left(J_4^{\gamma_m/2}-1\right)-\tilde{\mu}_m\ln J_4^{1/2}\right)$	$\sum_m\tilde{\mu}_m\geq 0,\ \tilde{\mu}_m(\gamma_m-2)\geq 0,\ J_4\geq 1$	yes
[4.] $\sum_j c_j\left[\frac{1}{\alpha_j+1}(J_4)^{\alpha_j+1}+\frac{1}{\beta_j+1}(K_1)^{\beta_j+1}+\frac{1}{\gamma_j}(I_3)^{-\gamma_J}\right]$	$c_j\geq 0,\ \alpha_j\geq 0,\ \beta_j\geq 0,\ \gamma_j\geq -\frac{1}{2}$	yes

[1.] see Holzapfel et al. (2000)
[2.] see Itskov and Aksel (2004)
[3.] see Markert et al. (2005)
[4.] see Schröder et al. (2008)